THESIS

# MODELLING AND SIMULATION OF COMBUSTION OF DILUTE SYNGAS FUELS IN A CFR ENGINE

Submitted by

Geet Padhi

Department of Mechanical Engineering

In partial fulfillment of the requirements

For the Degree of Master of Science

Colorado State University

Fort Collins, Colorado

Fall 2019

Master's Committee:

Advisor: Bret C. Windom

Daniel B. Olsen

David Dandy

ABSTRACT

MODELLING AND SIMULATION OF COMBUSTION OF DILUTE SYNGAS FUELS IN A CFR ENGINE

With increasing interest towards discovery of alternative fuels to act as sources of energy, many conventional internal combustion engines are being modified to operate on these new fuels. Optimization of engine specifications including compression ratio, intake/piston geometry, valve timing, and combustion phasing, can greatly improve performance when an engine is modified to operate on alternative fuels such as syngas and producer gas. However, the inability to predict the combustion characteristics of the alternative fuel, such as burn rates and auto-ignition conditions, is a significant challenge when simulation-based design of an engine is intended. The following thesis describes the development of a predictive model to simulate the combustion of a dilute syngas fuel in a Cooperative Fuel Research (CFR) spark ignited engine. The laminar flame speeds of the unique fuel mixtures calculated using CHEMKIN were coupled with the geometric features of the CFR engine to create a combustion model of the CFR engine in GT-POWER. Using two-zone modelling and detailed chemical kinetics, the model is also able to determine the performance of the engine along with any associated knocking tendency of the fuel and its corresponding operating conditions. Validation and tuning of the combustion parameters were performed through comparison to experimental pressure data taken from the CFR engine. The completed engine model can support the design and selection of operating conditions to maximize efficiency of other spark ignited internal combustion engines when powered by the dilute syngas fuel.

ACKNOWLEDGEMENTS

I would like to profusely thank my academic advisor, Dr. Bret Windom, for always supporting me through the course of the study and guiding me towards the right direction. He was always there to clarify my numerous questions and helped me get over several roadblocks which sprung up during the execution of the study. I am eternally grateful to him for giving me this chance and never losing confidence in me. I would also like to thank Dr. Dan Olsen and Dr. Todd Bandhauer for their constant support and insightful suggestions during the duration of the study. I would like to extend my acknowledgement to ARPA-E for financially supporting this study and awarding the grant number AR0000954.

I would also like to thank Alex Balu and Scott Bayliff for their help in providing me the experimental data needed for my work. I also want to thank Shane Garland and Matt Countie for their help throughout the study.

Finally, I would also like to thank my parents for their unwavering support and confidence in me. All of this could not have started without their role in it.

TABLE OF CONTENTS

# Chapter 1: Introduction

## 1.1 Motivation and Background

Ever since mankind has learned to create fire, different kinds of fuels have been explored to feed it. Initially, cellulose based fuels like wood were commonly used, primarily for heat generation and luminescence. Although abundant, wood did not burn very efficiently and released harmful substances such as soot when burnt. Also, due to its low energy density, large quantities of wood had to be used to generate the heat required by people. It is not surprising that with the discovery of fossil fuels like coal and petroleum, the preference of fuels quickly changed from wood-based sources to fossil fuels. This was because fossil fuels had higher energy densities and released less smoke than wood when combusted. With the advent of technology, the role of fuels changed from just providing heat and light to powering machines. One of the most commonly used machines for performing work is the internal combustion engine (ICE). ICEs harness the energy stored in the fuels like gasoline or diesel by combusting them in a closed piston-cylinder arrangement. The energy released by combustion pushes the piston outward and this motion can be converted into useful work. The applications of the ICE are numerous; ranging from power generation to transportation. In recent years due to increasing awareness about the depletion of fossil fuels and the negative environmental impacts of burning them coupled with the rising fuel prices, there has been increasing interest in the usage of alternative fuels. These alternative fuels can be cleaner and cheaper than the conventional fossil fuels. Examples of the alternatives include bio-fuels and natural gas. Natural gas, although a fossil fuel, can be considered as an alternative fuel to petroleum as it is not a commonly used to fuel ICEs, however, natural gas is highly abundant and thus has competitive pricing (on an energy basis) to petroleum fuels [1]. Also, natural gas is considered to have a cleaner combustion compared to conventional petroleum products due to its higher H to C ratio compared to the larger hydrocarbons found in petroleum derived fuels. These fuels, can be used alone in an ICE or can be blended with the conventional fuels leading to improved emissions and reduced fuel consumption relative to the conventional fuels [1, 2]. Other

substances which can be used as alternative fuels are syngas. Syngas (short for synthesis gas) can be defined as a mixture comprising of hydrogen, carbon monoxide, carbon dioxide and water and can sometimes include nitrogen and methane depending on the generation process used. The mixture has also been referred to as producer gas, especially when derived from gasified biomass. Although syngas contains hydrogen, which has a large heating value (119.7 MJ/kg), the presence of inert components like carbon dioxide, water, and nitrogen reduces the overall lower heating value (LHV) of syngas when compared to other fuels like natural gas. However, sources of syngas are numerous: by-products from biomass/digester plants, synthetic fuel generation, gasification of carbon containing substances, reforming higher hydrocarbons and tail gases from fuel cells. The large availability of this potential fuel alternative has promoted research on the feasibility of syngas to be used in ICEs [3, 4]. Mainstream application of these low heating value fuels in ICEs can help reduce fossil fuel dependency. Before any substance can fuel an engine, studies need to be done to understand and predict the combustion of the fuel and how the engine performs with that fuel. Characteristics such as heating values, energy density, flame speeds, engine power outputs, and combustion efficiency are some examples of the many factors considered to determine the usability of the fuel in the engine. Depending upon the fuel choice, the engine can also be modified to more efficiently convert the chemical energy into work. Modifications to an engine may include making changes to the compression ratios, operating speeds, piston crown geometry among many others. However, trying to gauge a prospective fuel's performance or to re-design an engine using only results from experimentation can be very tiresome and expensive. Data would have to be collected over multiple engine cycles with different operating conditions. Also, processing the huge datasets adds to the design time which is undesirable. With computers offering quicker solutions of complicated issues, it thus comes as no surprise that Computer Aided Engineering (CAE) techniques have become very popular during the design phase of many engineering applications in research circles and industry alike. Instead of laboriously trying to wade through large datasets gathered from physical experimentation, development of virtual models using CAE methods and running simulations on them greatly reduces the time and resources required to produce high fidelity results. This means the CAE methods now allow engineers to explore the feasibility of using different kinds

of substances as fuels in the ICEs. A prospective fuel can be extensively studied and then incorporated into virtual models of the engine. Multiple iterations on the virtual model can give an important head start in design processes before the experimentation on the actual engine is required. The current work focusses on developing a virtual model of the Cooperative Fuel Research (CFR) engine to study how using low heating value fuels, such as dilute syngas, affects the engine performance and determine the conditions in which the engine can operate safely. The results from this study can be used to support the computer aided engineering of new engines to operate on such dilute syngas.

## 1.2 Literature Review

### 1.2.1 Syngas operation in ICE's

Attempts to use low LHV fuels like syngas to generate energy is not a new phenomenon in the field of combustion. In the paper by Hagos et al., 2014 [4] the authors have mentioned that syngas from coal have been used for lighting purposes since the end of the $18^{th}$ century. In the 1920s a wood based syngas was also used for automotive applications and became popular during the Second World War when a gasoline shortage was experienced. Now, researchers have explored syngas for use in ICEs and gas turbines, especially due to its potentially cleaner combustion. For example, Chacartegui et al.,2011 [5] studied the emissions from various kinds of syngas when used in gas turbines. The syngas studied included gases derived from fossil fuels (e.g., gasified coal) and from biomass (e.g., gasified wood). The results from the study showed lower $NO_x$ emissions from the gas turbines when using syngas compared to using natural gas. Shah et al., 2010 [6] studied the performance and exhaust emissions of a spark ignited (SI) engine when run completely on a biomass based syngas. The syngas obtained for their research had a volume/volume% composition of 16.2-24.2% CO, 13-19.4% $H_2$, 1.2-6.4% $CH_4$, 9.3-13.8% $CO_2$ and the remaining $N_2$. This gas was produced by gasification of hardwood chips and had an average LHV of 5.79 $MJ/m^3$. This is quite low compared to the LHV of fuels such as natural gas which can range from 30 $MJ/m^3$ to 42 $MJ/m^3$ [7]. When comparing with the emissions from gasoline operation, the study found that the

syngas operation had lower CO and $NO_x$ in the exhaust. The comparison is shown in the FIGURE 1.1. Although the power output from the syngas operation was lower compared to the gasoline operation (due to the lower LHV of the syngas), the overall efficiencies of both fuels were similar at their respective maximum electrical power outputs.

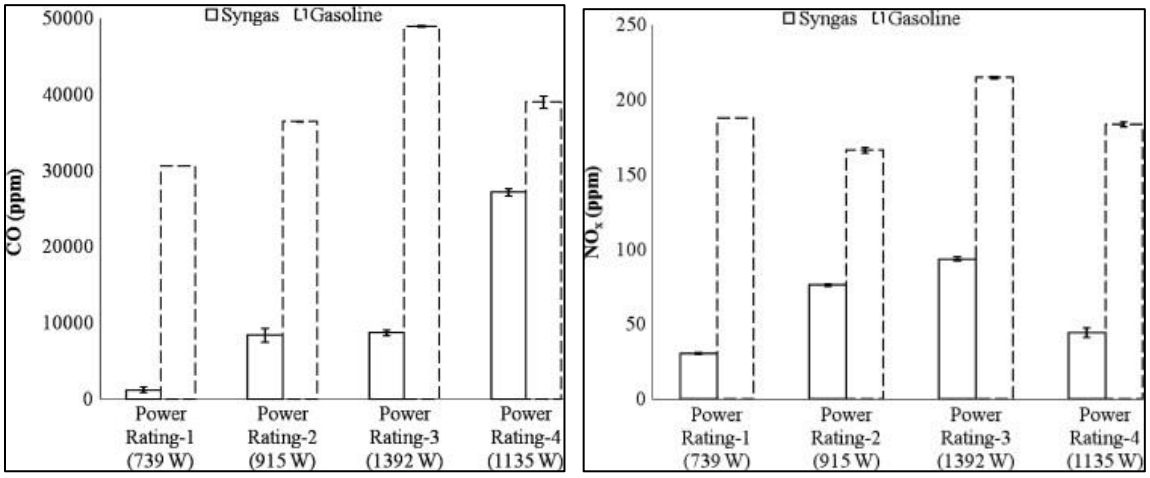


**FIGURE 1.1**: Exhaust emissions concentration of CO (left) and $NO_x$ (right) from generator for syngas and gasoline operations at different power ratings [6]

Studies have also been conducted on syngas being used in dual fuel compression ignition (CI) engines. Azimov et al., 2011 [8] investigated the effect of hydrogen and carbon dioxide contents in syngas on the performance and emissions of a dual-fuel engine. The study used operating conditions to allow premixed mixture ignition in end-gas region (PREMIER) combustion to have a two-stage heat release. PREMIER combustion occurs when a small amount of pilot fuel is injected and the energy release during initial stages of ignition leads to autoignition of the charge in the end gas region. Diesel was used to assist the autoignition of syngas in the study under lean condition for a wide range of equivalence ratios. The PREMIER combustion was observed enhancing the performance and increasing efficiency of dual fueling. Increased $H_2$ content led to higher combustion temperatures and efficiency, lower CO and hydrocarbon (HC) emissions but higher $NO_x$ emissions. Increased $CO_2$ content influenced performance and emissions only when it was increased to 34%. However, neither diesel could be completely substituted nor could syngas stand alone as a fuel in a diesel engine in the study. In the study by C.T.Spaeth at Queen's University,

Canada [9], a CI engine was modified to operate in dual fuel mode and the performance compared with either methane or syngas as the primary fuel. The syngas composition used was 10% $H_2$, 25% CO, 4% $CH_4$, 12% $CO_2$ and 49% $N_2$ by volume. The study concluded that the overall performance of the engine was better when methane was used instead of syngas in the dual fuel operation. But the exhaust emissions for CO and $CO_2$ was better for syngas than for methane at the same equivalence ratio. This is shown in FIGURE 1.2. Spaeth [9] also highlights that syngas operation could be a viable option due to its renewable nature, lower exhaust gas emissions and a larger operating range when compared to methane.

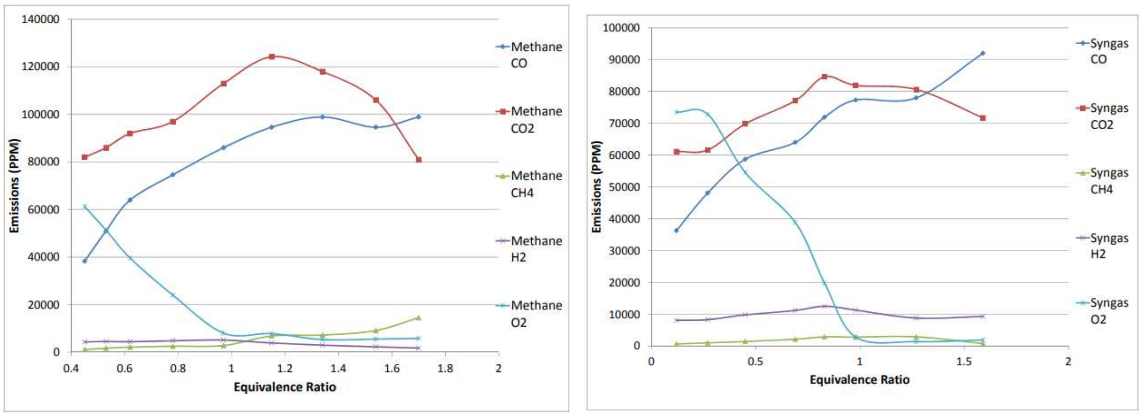


**FIGURE 1.2**: Emissions data for methane (left) and the syngas (right) when used with 5 % diesel pilot fuel in the CI engine [9]

### 1.2.2 CAE techniques

Combustion inside ICEs can be quite a complicated process to model and varies with the type of engine (e.g., SI engine or CI engine). For instance, in an SI engine the combustion is initiated by the energy of the spark whereas in a CI engine the combustion occurs due to the auto-ignition of the fuel injected. In both the cases the way the flame propagates inside the combustion chamber determines the burn rate of the inlet charge. In SI engines, the flame propagation in the engine plays a major role in the knock onset [10] and is affected by the turbulent flow inside the combustion chamber and the frontal area of the flame as it propagates into the unburned charge [11]. Additionally, in CI engines the spray characteristics of the injected charge greatly influences the CI combustion [12]. Also, parameters like cylinder and piston geometry, ignition delay of the fuel, and heat transfer inside the combustion chamber play important roles

in combustion in both the engine types (i.e, SI and CI). Using all the mentioned factors, an engine can be modelled to understand if an operating condition is prone to knocking or if maximum combustion efficiency can be attained. However, manually trying to model the engine taking all the relevant factors into account is extremely tedious and can sometimes be inaccurate under varying conditions of the engine. Using CAE techniques significantly reduces the labor required to understand and predict the behavior of the engine. CAE methods have often been used to model different systems in a variety of applications. Results of models developed from CAE techniques have often been comparable with results from experiments. In the current study, the software GT-POWER and CHEMKIN have been extensively used in the modelling process.

#### *1.2.2.1 GT-POWER*

GT-POWER is commonly used in engine research applications. GT-POWER is one of the leading engine and vehicle simulation tools used by engine makers and suppliers [13]. Developed by Gamma Technologies, GT-POWER is capable of 0D/1D modelling with built in structural and thermal 3D Finite Element Analysis (FEA). It also includes 3-D multi-body dynamics with flexible bodies and 3D Computational Fluid Dynamics (CFD) [14]. The available templates in the software used for describing different engine components and analytical techniques prove to be quite useful and have been used in previous studies. In the paper by McCrady et al., 2007 [15], the authors created a CI combustion model using GT-POWER to study engine performance and emissions of biodiesels derived from soybean and rapeseed. The authors used the in-built 'DI-Jet' combustion model in GT-POWER to handle both mixing and kinetic limited combustion as well as to provide a smooth transition between the two. The calibration of the engine model was done by matching the burn rate data provided by John Deere. Adjustments were made to control the air entrainments and the amount of fuel impinging into the piston bowl. By doing so, the authors were able to model the combustion of their biodiesel and thus have an estimate of the emissions from the engine. FIGURE 1.3 shows the calibration of the burn rate of the model by comparing with the default data provided to the authors.

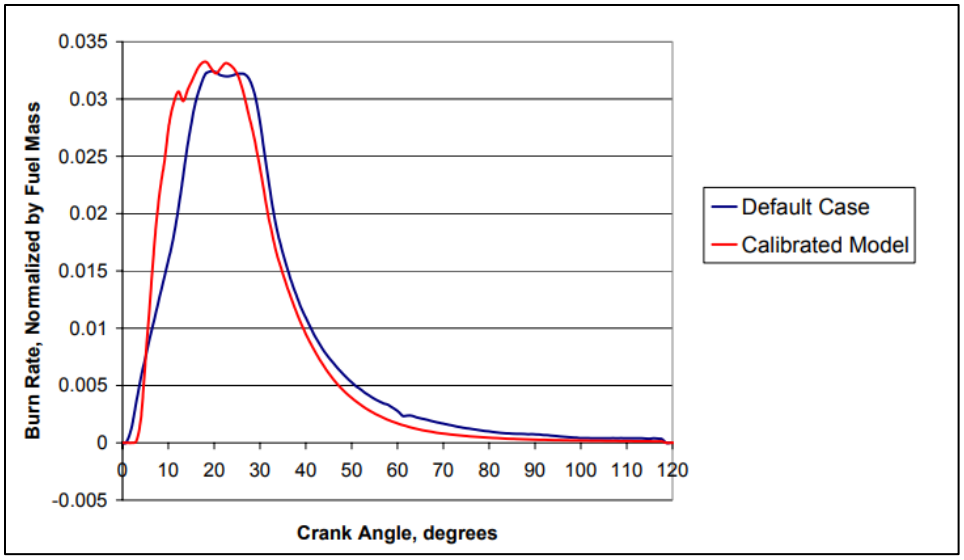


**FIGURE 1.3**: Calibration of burn rate in the model for high load condition.

Etheridge et al., 2007 [16] also used a GT-POWER model to validate their nitric oxides ($NO_x$) emissions predicted from a newly proposed probability distribution function (PDF). The PDF used a detailed chemical mechanism throughout the cycle and takes into account the mixing of the burned and unburned regions inside the engine. The GT-POWER model was then used to simulate the 'breathing' events of the engine during multi-cycle simulation. The conditions at inlet valve closing (IVC) were obtained as a result and used as inputs to their PDF for validation. The model was calibrated using previously documented emission results from a single cylinder research engine. A similar application of GT-POWER was shown by Noda et al., 2004 [17]. Noda indirectly coupled a one-dimensional engine model in GT-POWER with a zero-dimensional knocking simulation. The conditions predicted by GT-POWER at IVC are transferred to the knocking simulation mechanism to predict knocking in the engine at different operating points. The authors concede that directly incorporating the auto-ignition into the engine model would be a better way to conduct their transient knock simulation but mention the direct coupling would take too much CPU time and thus avoided that route. GT-POWER models have not only been used to provide inputs to chemical mechanisms but also to determine boundary conditions for other CAE software. In the paper by Pal et al. (2018) [18], a 3-D CFD code, CONVERGE, was used to develop a numerical model and perform the full cycle

simulations of the CFR engine for knock predictions. The boundary conditions used in the CFD model was obtained from the GT-POWER engine model also developed by the authors.

Of the available engine analysis methods in GT-POWER, the Three Pressure Analysis (TPA) method is a common choice for many studies. The TPA involves using high speed pressure data from the intake, exhaust and the in-cylinder pressures as inputs to the engine model. The simulation is run for multiple cycles until the model has converged. As a result, there is no requirement of residual fraction and trapping ratio as inputs to the model and instead are calculated from the TPA [13]. Further details of the TPA procedure are explained later in this thesis. In the paper by Choi et al., (2018) [19], the authors used the TPA model to estimate the conditions of the charge at IVC like residual gas fractions and gas temperatures. The TPA model is used to calculate these conditions by matching several other experimentally measured boundary conditions like mass flow rate of fuel and air and volumetric efficiency of the engine. By adjusting the heat transfer model of the TPA, Choi et al. were able to estimate the inlet gas temperature to an acceptable degree of certainty. A similar use of the TPA was done by Tsuchiyama et al. (2016) [20], in developing a model to predict the performance of a general purpose (SI) engine. The authors used an unsteady combustion speed equation that considered the transition from laminar combustion to turbulent combustion. As it is difficult to account for the influence of turbulence associated with the combustion chamber geometry and operating conditions, results from the 3-D simulation implemented in the CONVERGE CFD code were analyzed instead. The results that related to the in-cylinder flow and turbulence intensity were used in the 0-D combustion model to describe the effect of flow speed and turbulence on the turbulent flame speeds. The validation of the heat transfer models was done using the usual approach by comparing the model results with the experimental results.

#### *1.2.2.2 Predictive modelling*

Modelling using computer simulations is also used in predictive analysis in situations where computationally ‘expensive’ methods are not desired. A well calibrated model has often been used in studies to predict engine combustion and overall performance. In a paper by Kulkarni et al. (2010) [21] the

authors used GT-POWER to develop a whole-engine model of a Cummins 2007 turbocharged diesel engine. They developed the model to give a detailed representation of the diesel engine components such as the intake and exhaust manifolds, valves, multi-pulse injectors, cylinders, turbochargers and cooled EGR loop. The predictive combustion model 'DI-Jet' is then used to calculate the in-cylinder heat release, temperature and species concentrations. The authors then calibrated the model by comparing the predicted parameters at different operating points like combustion rate multiplier and compressor efficiency multiplier with the nominal values for the engine at those points. The authors made slight changes to the model inputs like the in-cylinder heat convection, convection efficiency, and combustion rate to match the nominal values. After the calibration, the authors found the predictions for parameters like heat release, airflow and key combustion performance outputs like brake specific fuel consumption (BSFC), peak cylinder pressure (PCP) and net mean effective pressure (NMEP) satisfactory. A slightly different method for developing the predictive model was shown in the Master's thesis by M.C. Hulbert at the Illinois Institute of Technology [7] . Hulbert worked on developing a model for a dual fuel combustion simulation model for a 2 liter 4-cylinder common rail direct injection (CRDI) diesel engine with EGR. The model was developed and validated using data from an in-line heavy duty 6-cylinder dual fuel engine at the Argonne National Labs (ANL). As the focus was on understanding the combustion process, the model was simplified to a single cylinder engine simulation. To model the dual fuel combustion, Hulbert used two sub-models: one for diesel injection (DI) combustion and the other for SI combustion. The DI and SI combustion rates were then calculated by employing the TPA method. After that, the Measured + Predicted (M+P) Analysis model set up by GT-POWER was used to calibrate the model using experimental data. FIGURE 1.4 shows the results simulated by the model after the optimization. The model was then used to explore the effects of varying natural gas compositions on dual fuel combustion.

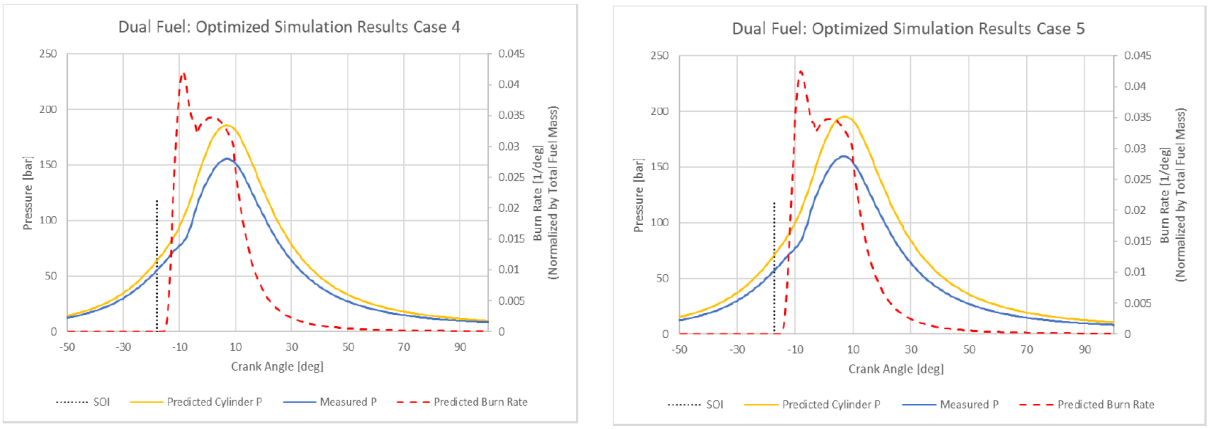


**FIGURE 1.4**: Optimized dual fuel simulation results from the model [7]

### *1.2.2.3 CHEMKIN*

GT-POWER has existing libraries to model engine operation using conventional fuels (e.g., gasoline, diesel). However, for combustion of custom fuels (e.g., syngas) in engines, GT-POWER requires additional information about the flame speeds. CHEMKIN was used to obtain this additional information. The 1-D software CHEMKIN is commonly used in research pertaining to combustion of materials. CHEMKIN, owned by ANSYS, is quite useful in creating combustion models of different types of fuels and in studying their associated parameters. In the paper by Natarajan et al., 2009 [22], the experimental results of the laminar flame speeds calculations for different compositions of $H_2/CO/CO_2/O_2/He$ at high pressures are compared with the values from a CHEMKIN model developed by the authors. Wang et al., 2012 [23] investigated the laminar flame speeds of typical bituminous coal derived syngas by employing the Bunsen flame approach. The experimental results were compared with the results of two chemical kinetics simulations predicted in CHEMKIN. The focus of the paper was to estimate the flame speeds with varying concentrations of hydrogen ($H_2$) in the syngas. A similar study was also done by Das et al., 2011 [24] focusing on the effect of the water and carbon monoxide (CO) concentrations on flame speeds of a syngas. The authors used the chemical mechanism developed by Li et al. [25]. FIGURE 1.5 shows the validation of the data obtained from CHEMKIN against the data obtained from literature. The term $\eta_{H2/CO}$ represents the ratio of $H_2$ to CO in the mixture. The results from the developed CHEMKIN model were compared with experimental data for a wide range of $H_2$/CO ratios and equivalence ratios ($\phi$) along the effect of water

addition on the laminar flame speeds was studied. It was shown that for small $H_2$/CO mixtures adding water increases the laminar flame speeds until a critical water concentration percentage. Beyond that limit the flame speeds begin to decrease. This is shown in FIGURE 1.6. For higher $H_2$/CO concentrations, the laminar flame speeds steadily decrease with increase in water. This trend is illustrated in FIGURE 1.7.

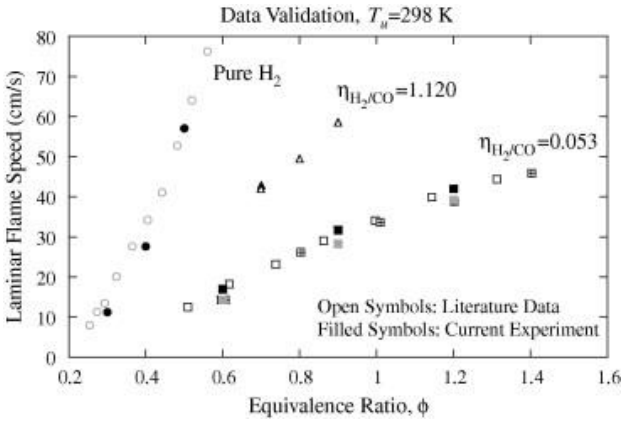


**FIGURE 1.5**: Data validation of CHEMKIN results

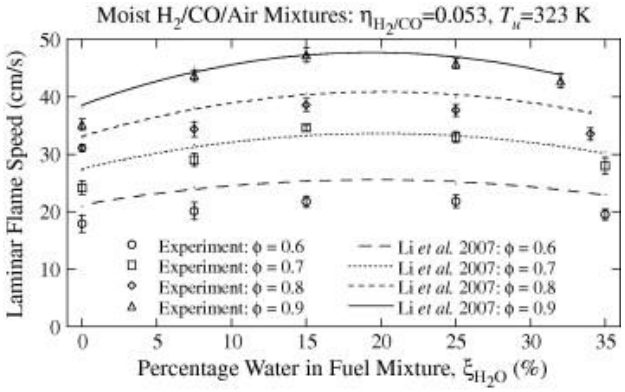


**FIGURE 1.6**: Variation of laminar flame speeds with water addition for $\phi$ = 0.6, 0.7, 0.8, and 0.9, $\eta_{H2/CO}$ = 0.053, and unburnt temperature of 323 K

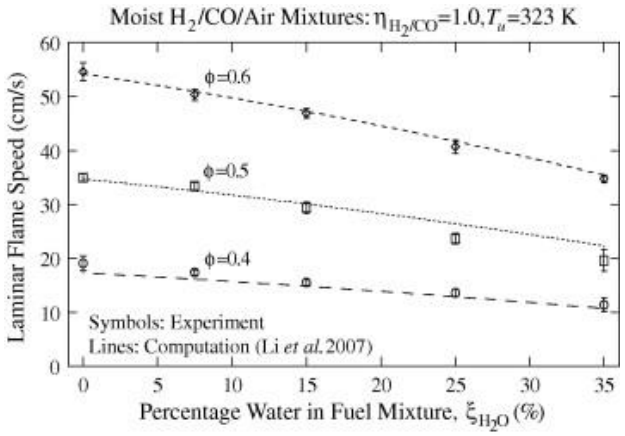

**FIGURE 1.7:** Variation of laminar flame speeds with water addition for $\phi$ = 0.4, 0.5, and 0.6, $\eta_{H2/CO}$ = 1, and unburnt temperature of 323 K

### *1.2.2.4 The Wiebe function*

Prediction of engine parameters when using any fuel can be carried out by solving the physics at each point in the control volume of the engine using CAE methods or by utilizing established correlations that connect the output with the conditions in the engine. The Wiebe function is such an empirical correlation used for determining burn rates in engines and has often been associated with predictive combustion modelling [26]. The commonly used form of the Wiebe equation is shown in eqn. 1.1 and defines the fuel mass fraction burned as a function of crank angle [26, 27]:

$$x(\theta) = 1 - \exp\left[-a\left(\frac{\theta-\theta_i}{\Delta\theta}\right)^{m+1}\right] \quad \text{…Eqn. 1.1}$$

Coefficient *a* is directly related to the combustion duration [28], while coefficient *m*, known as chamber shape factor, models the propagation flame front [27]. $\theta$ refers to the crank angle degree and $\theta_i$ refers to angle at the start of ignition. This equation has also been used in other different forms, based on the requirement of the authors [26]. The values of *a* and *m* differ based on the fuel and type of engine used. However, standard fuels like gasoline diesel and natural gas have well defined values for these coefficients for spark-ignition and compression-ignition engines [27] that correlate well with experimental data. In the paper by Borg et al. (2008) [29], the authors estimate the heat release consumed and the mass of fuel burned by auto-ignition in a gasoline fueled SI engine. The authors used the Wiebe function in a slightly different form than that of eqn.1.1 and determined the rate of heat release as it is proportional to the rate of mass burned fraction. The authors first used optimization schemes to fit the Wiebe function to the data from individual non-autoigniting combustion cycles. Then, the Wiebe function was trained to fit the heat release of individual cycles using only partial combustion data. By inputting the combustion data from auto-ignition cases till the start of knocking, the authors were then able to determine the heat release that would have occurred in the absence of knock. The difference in the measured and calculated heat release allowed them to predict the heat lost due to knocking. Kalghatgi et al. (2005) [30], also used the Wiebe function to develop

an empirical model for SI combustion. The authors also used existing correlations of laminar burning velocity as a function of pressure, temperature, air-fuel ratio and residual gas content to predict the relative change in the Wiebe parameters. These correlations for the laminar flame speeds are employed in the current thesis and are explained in detail in the later chapters. By using the correlations, Kalghatgi et al. were able to reduce the calibration data needed for the combustion model. To account for the turbulence in the engine, the authors have used additional correlations of engine speed and spark timing parameters and mention the turbulence related correlations must be calibrated to the specific engine. Although predictive in nature, the authors agree their model would not be able to predict knock as knock is not associated with the average combustion event. Knock is the fastest burning cycles that give the highest temperatures and pressures in the cylinder. The authors do suggest developing a correlation to account for the cycle to cycle variation in the Wiebe parameters in a similar way as the combustion correlation developed by them would allow knock predictions in the 1-D simulations.

## 1.3 Deficiencies in literature

Syngas is a very broad term for a category of gases used in the synthesis of other products. Syngas is usually a mixture of hydrogen and carbon monoxide gases and can be diluted by different species like carbon dioxide or water. This can lead to syngas having different compositions based on the application and source of the gas and thus different combustive behaviors. Even the studies done on combustion of alternate or low LHV fuels have used gases of varying compositions based on the sources. It is thus extremely difficult to find previous works that have used the exact composition of the syngas to be used in this current study. This makes the task of understanding the combustion parameters of the syngas, such as flame speeds, just based on previous studies almost impossible. Also, since the current study is interested in more than one blend of the syngas, using a generic model for syngas explored in previous studies is inadequate for predictive modelling purposes. So, the method of using CAE techniques (CHEMKIN or GT-POWER) for the combustion analysis of various syngas mixtures being considered was a viable solution for this study.

Development of predictive combustion models using correlations like the Wiebe function is often observed for conventional fuels like gasoline and diesel. The coefficients of the Wiebe function for those fuels is well documented in the literature, thanks to the numerous experiments done in previous studies. But those coefficients rely heavily on the fuel being used. An uncommon kind of fuel, like the syngas mixture used in the current study, has no prior documentation of Wiebe coefficients. As a result, using empirical correlations like the Wiebe function becomes difficult. In order to be able to use such correlations additional experiments detailing the combustion properties of the fuel would need to be carried out, which would require an additional expense of time and money. The other computationally inexpensive means of developing a predictive model would be to use a 1-D modelling code. Many studies rely on 1-D modelling programs, such as GT-POWER, to get the initial conditions of the engine at the IVC through methods like the Three Pressure Analysis. These values are either used as the boundary conditions for other multi-dimensional modelling software like CONVERGE, to predict the combustion in the engine or used as inputs to detailed chemical mechanisms developed by the authors. Works that involved usage of 1-D modelling codes for development of predictive combustive models, like the one by Hulbert [7], did not directly couple the chemical kinetics into the modelling code. Directly coupling the chemical kinetics can allow for faster computation and has been explored in this current study. Also, development of a predictive model for knock for a multi-component low LHV syngas has not been explored by many researchers. The current study focusses on developing a predictive combustion model with knock detection for a dilute non-conventional fuel (or a syngas) with low LHV using the 1-D modelling software GT-POWER.

## 1.4 Objectives

The remainder of this thesis will describe the work done towards addressing the following objectives:

- Setting up the CFR engine to conduct experiments and gather data needed to support model development. This was conducted by another graduate student.

- Understanding the effect of syngas composition on the combustion of the mixture and using the data to aid the development of a combustion model.
- Creating a virtual model of the CFR engine and developing a combustion model of the engine running on the syngas.
- Calibrating the combustion model with experimental data to develop a predictive combustion model capable of predicting the performance and knock onset/magnitude in the engine when using the dilute syngas as fuel.

## 1.5 Thesis Organization/Overview

The thesis is organized into different chapters with multiple sub-sections:

- Chapter 2 describes the experimental setup used to collect test data to support model development. This includes specifications of the engine used, arrangement of associated flow lines, details on sensors used and the data acquisition techniques adopted in the experiment.
- Chapter 3 explains the numerical modelling and CAE software implementation in the study. Details on the factors considered while modelling the engine and methods used to determine the combustion parameters of the syngas are explained. Considerations chosen during the development of the simulation model and its associated components are also described.
- Chapter 4 shows the results of the predictive modelling and discusses the validation techniques used to verify the predictive nature of the model through comparison with experimental data.
- Chapter 5 discusses the next steps and possible improvements to the model along with the suggested means to achieve them.

# Chapter 2: Experimental setup

## 2.1 The CFR engine

The Cooperative Fuel Research (CFR) F1/F2 engine (FIGURE 2.1), due to its unique features and setup, was chosen to run the syngas mixtures considered in this study. The exterior of the cylinder has a worm gear to raise or lower the cylinder relative to the piston/connecting rod assembly. This causes the clearance volume to change, thus adjusting the compression ratio of the engine during operation. Due to this feature the CFR engine is commonly used in studies to determine the octane number of fuels. The CFR engine is also robustly built to withstand large/rapid pressure fluctuations like the ones caused by engine knock [31]. These features are particularly useful when trying to determine the operating range of the engine when running on a fuel which has limited prior documentation about its knock limit and operating envelope. TABLE 2.1 shows the main specifications of the CFR engine present at Colorado State University [32].

**TABLE 2.1:** CFR engine specifications

| | |
|---|---|
| Combustion chamber | Cast iron, flat 'pancake' |
| Compression ratio | Adjustable, 4:1 – 18:1 |
| No. of cylinders | 1 |
| Bore X Stroke (mm) | 82.55 X 114.3 |
| Displacement ($cm^3$) | 611.7 |
| Connecting rod length (mm) | 254 |
| Fuel system | Carbureted |
| Ignition | Capacitive discharge coil to spark |

The CFR engine at Colorado State University had a knockmeter sensor installed in the cylinder head to detect knock in the engine. To place the knockmeter a cavity had to be drilled in the cylinder wall of the engine and can be seen in the FIGURE 2.2. Currently, the knockmeter has been replaced with a Kistler Type 6061B high speed piezoelectric pressure transducer. The pressure transducer allows the collection of the crank angle resolved in-cylinder pressure during engine operation which is required to perform the Three Pressure Analysis (TPA) explained later. The inlet pressure to the engine is measured using a piezoresistive Kistler Type 4007D-DS pressure sensor. The exhaust pressure of the engine is measured by

a piezoresistive Kistler Type 4049B-DS pressure transducer. The positions of these pressure transducers are illustrated in FIGURE 2.2. The inlet and exhaust pressure sensors are absolute pressure sensor whereas the in-cylinder pressure transducer is a dynamic pressure sensor. Dynamic pressure transducers, unlike absolute sensors, do not measure pressure as values off an absolute scale at any point of time. Instead, they measure the transient pressures changes between two states in the system. Thus, to ensure the dynamic sensor gives correct values of pressure on an absolute scale, it needs to be pegged to a known pressure first. In the experimental setup used, the pegging of the sensor is done to the absolute value pressure transducer in the buffer volume at a crank angle of 175 degrees before top dead center (BTDC).

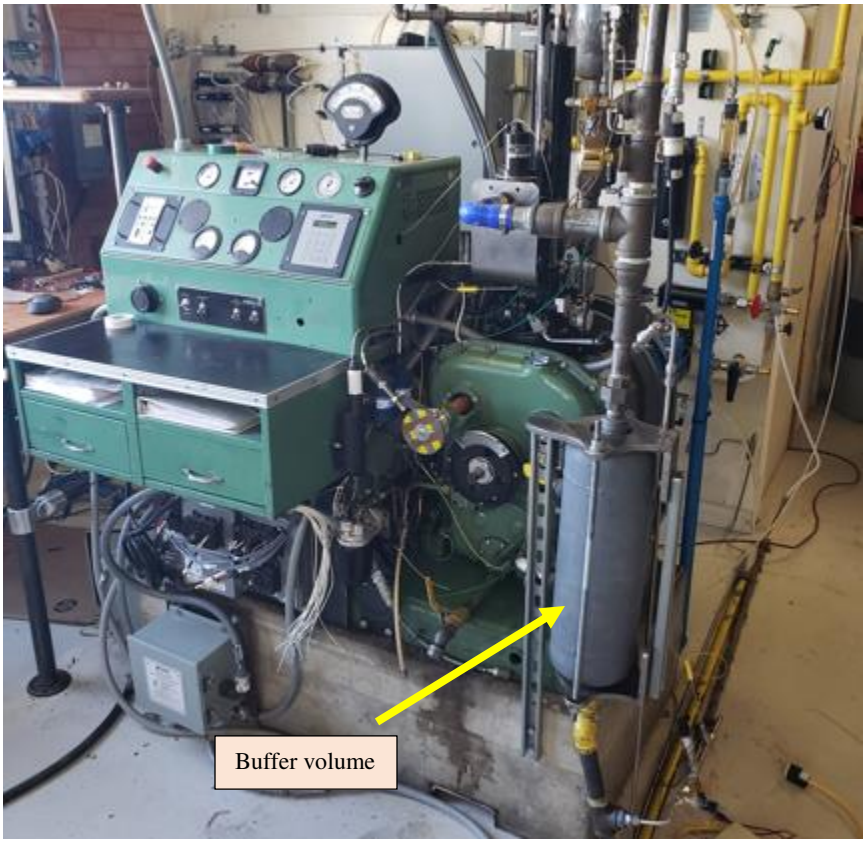


**FIGURE 2.1**: Picture of the CFR engine at the Powerhouse facility of Colorado State University

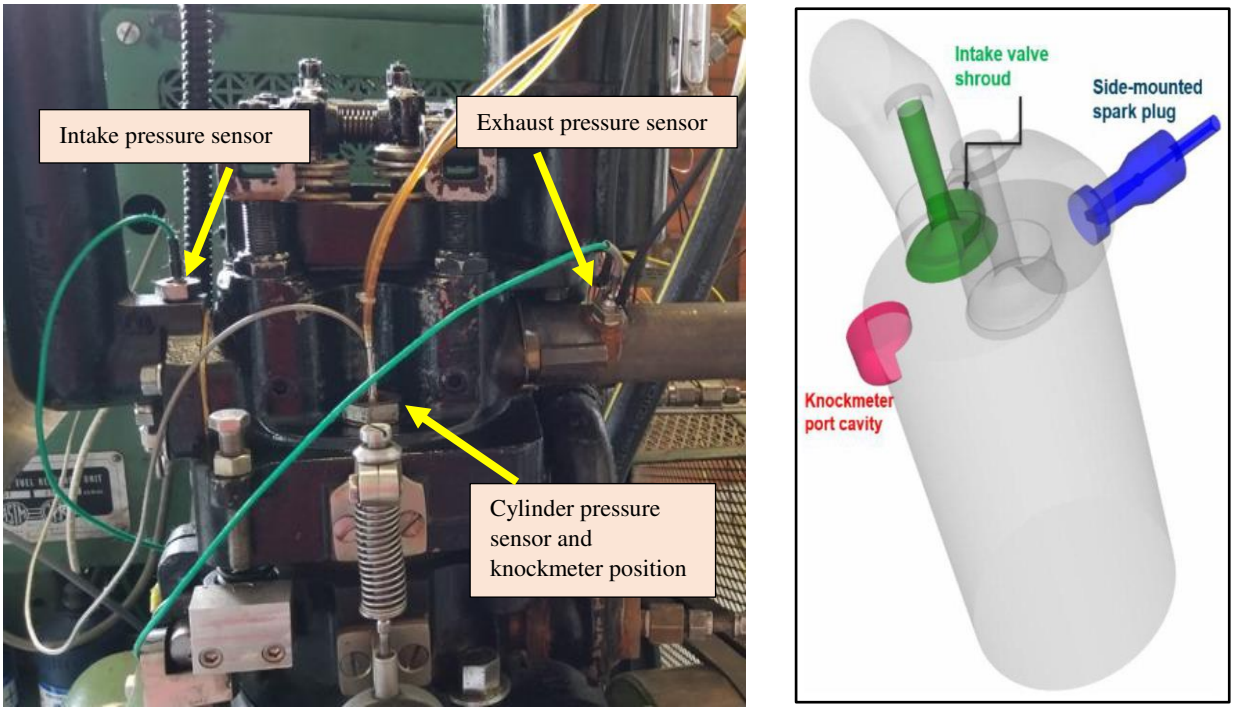


**FIGURE 2.2**: Image of the CFR head with sensor positioning (left). Image of the knockmeter cavity below the knockmeter (right) in the CFR engine.

To detect the intensity of knocking in an engine, a knock index (KI) was defined. The KI allows to correlate knocking and the scale of damage that can be caused due to it and depends on the engine type, sensor placement, engine load, and operating conditions. The value of KI can be calculated by using heat transfer analysis in the engine or in-cylinder pressure analysis [33]. For calculation of the KI in the CFR engine, a Fast Fourier Transform (FFT) was used on the data from the in-cylinder pressure readings. This resulted in pressure amplitudes in the frequency domain produced by abnormal combustion such as auto-ignition. A band-pass filter was then applied to the real-time pressure data to remove noise and get the peaks in pressure. The experiment used the maximum FFT amplitude of a knocking engine cycle as a reference to establish knock levels. The KI was then defined as the summation of the maximum FFT amplitudes of the last 200 engine cycles [34]. In this study, cases having a KI of greater than 300 were considered as consistent knocking cases. FIGURE 2.3 shows examples of the output from the FFT at different engine operating conditions and their corresponding KIs. Higher KI conditions can be seen to have higher frequency of the pressure amplitude peaks. Higher pressure amplitude corresponds to greater engine knock during a cycle.

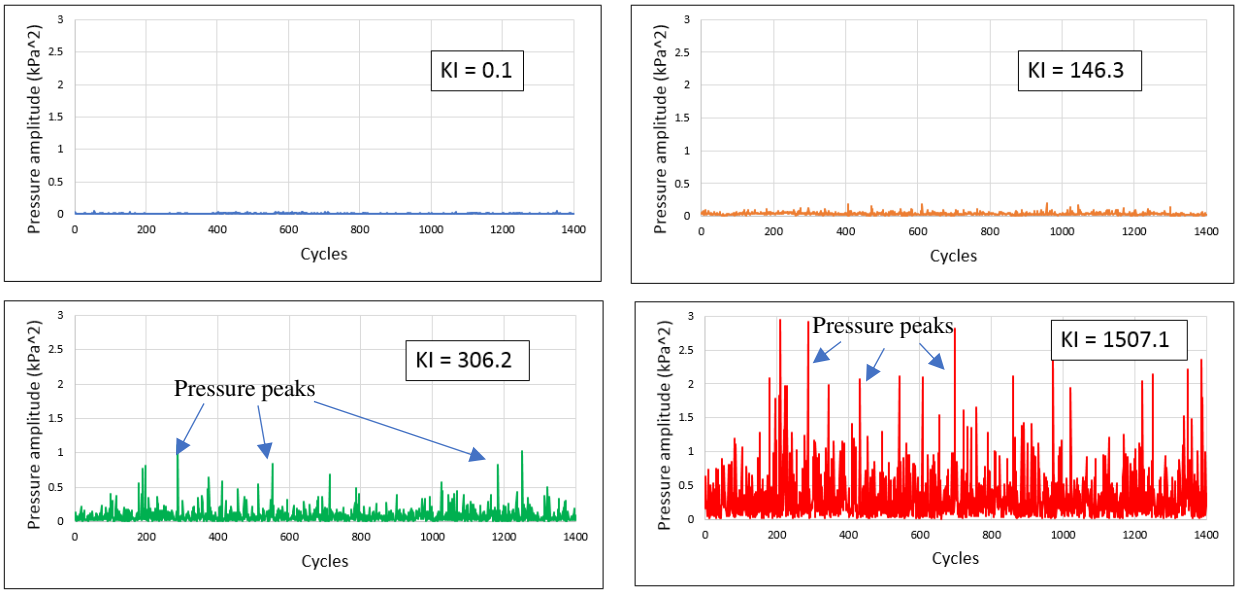


**FIGURE 2.3**: Illustration of pressure amplitudes obtained from different engine operating conditions by the FFT method for different KI in the CFR engine.

## 2.2 Stock Syngas Mixture

The syngas explored in this study is from the exhaust tail-gas of a solid oxide fuel cell (SOFC) originally fueled by natural gas and being currently developed in a separate project [35]. The SOFC tail-gas consists of a mixture of hydrogen, carbon monoxide, methane, carbon dioxide and water in varying percentage compositions. TABLE 2.2 shows the stock composition of the tail-gas. The heating value of the stock composition of the fuel is about 2.6 MJ/kg and a low stoichiometric air-fuel ratio of 0.72. The heating value is significantly low when compared to the other fuels like gasoline (44.5 MJ/kg) and natural gas (50 MJ/kg) [36]. The stoichiometric air-fuel ratio for gasoline is 14.59 and for natural gas is 16.79 [37] which are significantly higher than the stock tail-gas being considered.

**TABLE 2.2**: Stock composition of the tail-gas considered in the current study

| Constituent | Composition (molar %) |
|---|---|
| Hydrogen ($H_2$) | 17.7 |
| Carbon Monoxide (CO) | 4.9 |
| Methane ($CH_4$) | 0.4 |
| Carbon Dioxide ($CO_2$) | 28.3 |
| Water ($H_2O$) | 48.7 |

To get the desired compositions of the syngas the individual constituents, except the water, were sourced from compressed gas bottles. The flow rates from the gas bottles were first measured using an Omega FMA Class 1700 mass flowmeter. A rotameter was used to manually adjust the mass flow of the individual gases according to the calculated mass flow for the required syngas mixture. The individual gases were then mixed together in a manifold with the combined flow regulated using a Pulse Width Modulation (PWM) controller. The flow of this combined gas mixture blend was checked using a Coriolis flowmeter. FIGURE 2.4 shows the flowmeters used in the experiments. The fuel was then mixed with air and additional carbon dioxide in the buffer volume chamber (shown in FIGURE 2.1). Additional carbon dioxide was input in the stream to match the composition of the desired mixture to be tested. The air used in the experiment was the shop air which is dehumidified and pressurized to 160 psi in the basement of the facility. A regulator throttled down the air to 90 psi before usage in the experiment. An Omega FMA Class 1744 flowmeter was used to control the mass flow rate of the air being used. After the mixture of air and syngas exited the buffer volume, superheated steam from a steam generator was added to the stream to match the water content in the inlet composition desired to enter the engine. The intake manifold was wrapped with heat tape to prevent condensation of the steam in the inlet stream. K-Type thermocouples were attached below the location of the pressure sensors for the intake and exhaust ports of the engine and also in the buffer volume chamber to record the respective gas temperatures. All this data of gas pressures and temperatures was recorded in real time using the LabVIEW software. The experiments were conducted by targeting an average indicated mean effective pressure (IMEP) of 850 kPa. The experimentally recorded data was then processed resulting in a crank-angle resolved manner which is used in the numerical modelling.

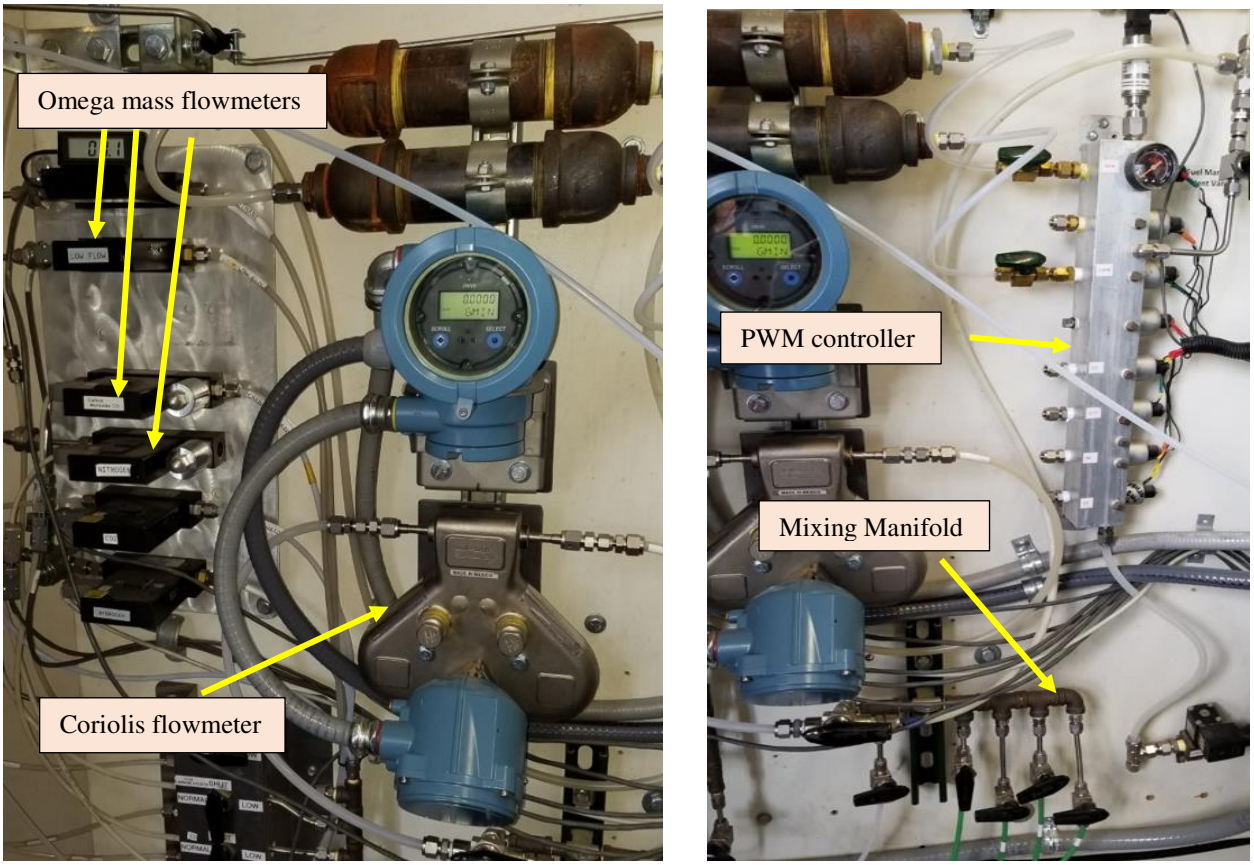


**FIGURE 2.4**: Images of the flow meters used in the CFR engine setup

# Chapter 3: Numerical Modelling

The overall sequence of steps followed for the numerical modelling in this study can be illustrated in FIGURE 3.1. These steps can be broadly divided under the following categories: syngas blends analysis, GT-POWER modelling, and CHEMKIN modelling. Each division is discussed in the subsequent sections.

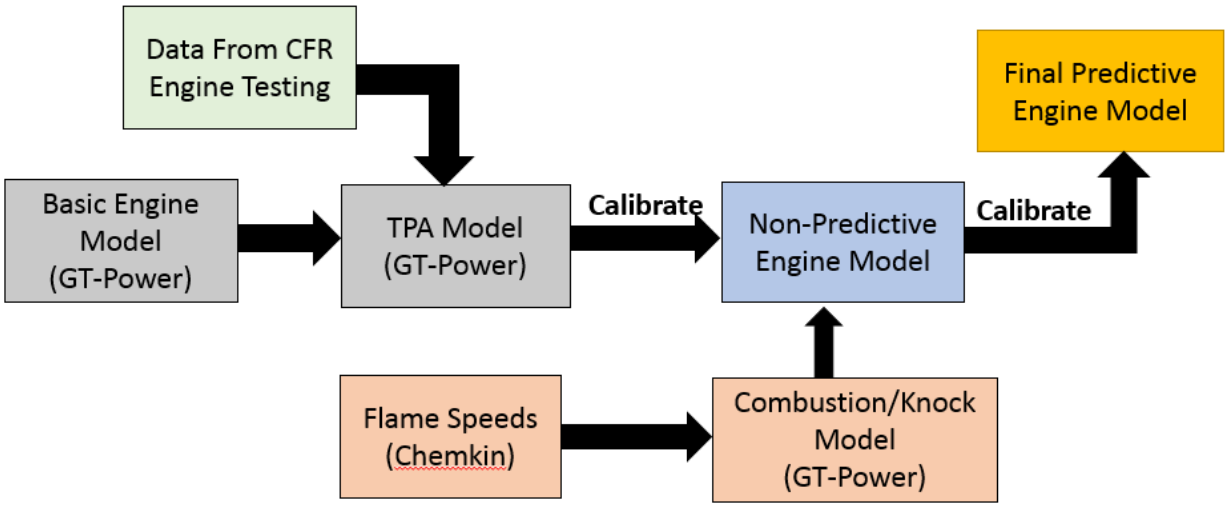


**FIGURE 3.1**: Overall steps involved in the development of the predictive model of the CFR engine.

## 3.1 Syngas Blends

One way to increase the heating value of the fuel is to increase the composition of flammable gases, like $H_2$ and CO, in the mixture. This can be done by cooling the stock syngas mixture to condense out water from it. As the current study does not receive the syngas mixture from an actual fuel cell and instead uses compressed gas bottles to fabricate the blend, it is necessary to know what kind of constituent composition must be mixed to get the desired blend. To determine the composition of the mixture after the water dropout, the concept of vapor pressure of water and relative humidity was used. Eqn. 3.1 shows the formula used to determine vapor pressure of water.

$$P_{water} = \phi * P_{sat@T} \quad \text{…Eqn. 3.1}$$

where, $P_{water}$ is the vapor pressure of water, $\phi$ is the relative humidity and $P_{sat@T}$ is the saturated vapor pressure of water at any temperature ($T$). This study uses the values of vapor pressure of water at different temperatures from the National Institute of Standards and Technology (NIST) [38]. FIGURE 3.2 shows the water vapor pressure reported by NIST.

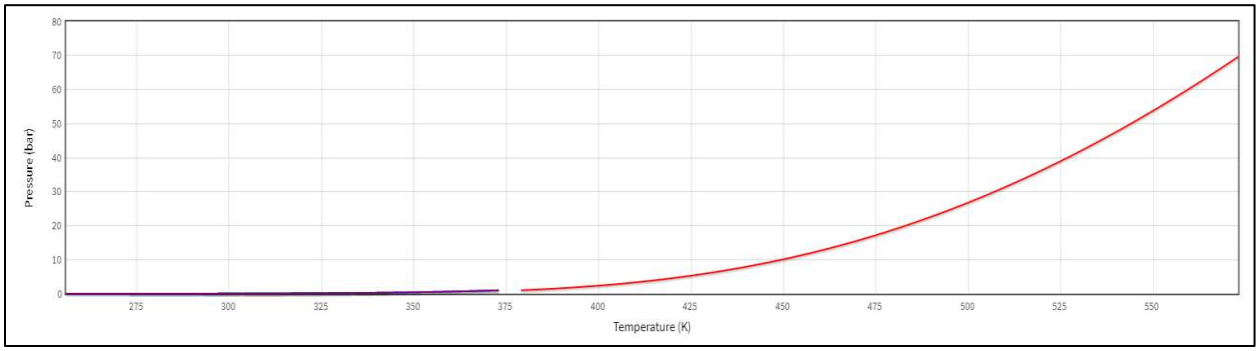


**FIGURE 3.2**: Curve used to find vapor pressure of water at different pressures and temperatures.

The value of $\phi$ cannot exceed 1 as the condition of $\phi$ =1 represents a completely saturated gas. At this value the partial pressure of water should be equal to the saturated vapor pressure of water at that temperature. The partial pressure of water ($P_{water}$) in the syngas mixture can be calculated by using the eqn. 3.2.

$$P_{water} = \chi * P_{total} \quad \text{... Eqn. 3.2}$$

where, $\chi$ is the mole fraction of water in the mixture and $P_{total}$ is the total pressure exerted by the syngas mixture. In this case, the tail-gas exits the fuel cell at a pressure of 3 bar and the same is replicated in the calculations to find the mixture composition. So, the total pressure $P_{total}$ was set to 3 bar. Once the partial pressure of water ($P_{water}$) from eqn. 3.2 becomes greater than the vapor pressure obtained from eqn. 3.1, condensation of the water will occur until the two pressures become equal. This allows for the determination of the new mole fraction of water in the new syngas mixture after the water dropout due to condensation. The relative composition of the remaining gases remain unchanged as only the water is removed from the mixture. The new composition of the syngas can thus be calculated by increasing the composition of the other gases by the fractional decrease of water composition with respect to the remainder of the gases. Eqn. 3.3 and eqn. 3.4 show the calculations used.

$$Reduction\ in\ water\ (mole\ fraction) = \Delta\chi = \chi_{old} - \chi_{new} \quad \text{… Eqn. 3.3}$$

$$Increase\ of\ other\ gases\ (mole\ fraction) = \chi_{gases}' = \chi_{gases} * (1 + \frac{\Delta\chi}{1-\Delta\chi}) \quad \text{… Eqn. 3.4}$$

where, $\chi_{gases}$ represents the mole fraction of the gases other than water in the stock composition of the syngas, $\chi_{gases}'$ denotes the new mole fractions of the gases in the syngas after the water dropout. Based on the specifications of the fuel cell development project [35], 40°C was determined as the lowest temperature which the intercooler could attain. This would thus be the lowest temperature that the syngas could be cooled to. It was then decided to explore the modelling of the syngas when cooled to three different temperatures: 40°C, 60°C and 90°C. The new compositions of the syngas at the mentioned cooling temperature are shown in the TABLE 3.1 to 3.3. In this study the composition of the syngas at the 40°C water dropout is referred to as Blend 1, the composition at 60°C dropout is referred to as Blend 2, and the composition at 90°C water dropout as Blend 3. It can be observed that the compositions of Blend 1 and Blend 2 are quite similar. Thus, to save computation time, this study decided to focus only on Blend 1 and Blend 3.

**TABLE 3.1**: Composition of syngas when cooled to 40°C (Blend 1)

| **Constituent** | **Composition (Molar %)** |
|---|---|
| Hydrogen ($H_2$) | 33.65875 |
| Carbon Monoxide (CO) | 9.31796 |
| Methane ($CH_4$) | 0.76065 |
| Carbon Dioxide ($CO_2$) | 53.81597 |
| Water ($H_2O$) | 2.446667 |

**TABLE 3.2**: Composition of syngas when cooled to 60°C (Blend 2)

| **Constituent** | **Composition (Molar %)** |
|---|---|
| Hydrogen ($H_2$) | 32.21952 |
| Carbon Monoxide (CO) | 8.919528 |
| Methane ($CH_4$) | 0.728125 |
| Carbon Dioxide ($CO_2$) | 51.51483 |
| Water ($H_2O$) | 6.618 |

**TABLE 3.3**: Composition of syngas when cooled to 90°C (Blend 3)

| Constituent | Composition (Molar %) |
|---|---|
| Hydrogen ($H_2$) | 26.4642 |
| Carbon Monoxide (CO) | 7.326248 |
| Methane ($CH_4$) | 0.598061 |
| Carbon Dioxide ($CO_2$) | 42.31282 |
| Water ($H_2O$) | 23.29867 |

## 3.2 GT-POWER Modelling

In order to better understand the dynamics of the experimental engine, a virtual model was developed using GT-POWER. Components like intake and exhaust manifolds and engine runners, which are not directly connected to the engine, were not explicitly described in the model. Instead, the end-effects of such entities were measured and implicitly included in the described components of the model. This ensured the focus of the study remained on the combustion modelling of the syngas mixture and not too much effort was spent on the auxiliary units. Using fewer components with fine details also reduces the computational effort needed by the software while running simulations. FIGURE 3.2 shows a screenshot of the CFR engine model developed in GT-POWER. The subsequent sections explain the model components used and the factors considered while developing them.

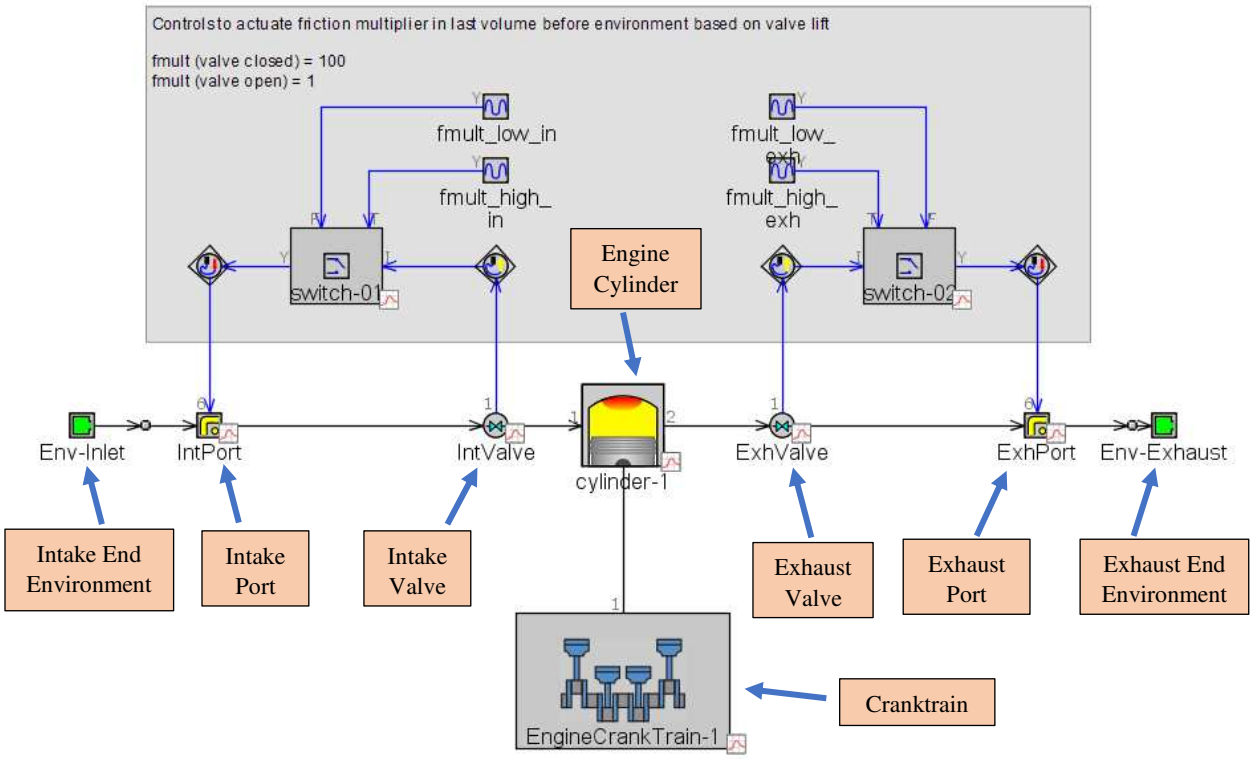


**FIGURE 3.2:** Model of the CFR engine developed in GT-POWER

### 3.2.1 Modelling engine components

#### *3.2.1.1 End Environment*

The 'EndEnvironment' component in GT-POWER is normally used to describe the boundary conditions, including the intake and exhaust pressure, temperature and composition. Additional inputs can include options to account for effects of altitude and humidity. While performing a Three Pressure Analysis (TPA), the 'EndEnvironmentTPA' component can be used to include the intake pressures for the analysis. In the simplified model these components are used to describe the conditions just upstream of the intake port and just downstream of the exhaust port. Here, the EndEnvironment objects essentially account for the runners and the intake/exhaust piping of the engine. The temperatures specified in the EndEnvironment component were taken from the thermocouples placed just before the ports on the runners. The intake and exhaust pressures used were recorded using the pressure transducers placed near the intake and exhaust ports of the engine respectively.

In the EndEnvironment component the composition of the gas going into the engine through the ports is defined. For direct injection engines this composition is usually just the air as the fuel is injected directly into the combustion chamber. However, the intake to the CFR engine is a premixed mixture of air and the fuel blend in a stoichiometric ratio. During the modelling process, a reporting bug in GT-POWER was discovered regarding the definition of the inlet composition. In operating conditions, such as that of the CFR engine, the inlet composition is usually defined using the object 'FluidMixture'. This object defines the mixture as a simple combination of the individual gases present. However, since the mixture used in this study has non-combustive components such as $CO_2$ and water in significant concentrations, the software identifies these components as part of the inlet air instead of being part of the syngas blend. This disrupts the air-fuel ratio and the intake air quantity reported by the software. TABLE 3.4 shows the difference in inlet charge to the engine modelled by the software for an operating point when using the FluidMixture definition. The mass of air and fuel entering the engine reported by the model shows discrepancy from the measured values due to the reason explained earlier. However, the total mass of inlet charge reported by the model is within 5% of the measured value. However, the thermal and fluid calculations appeared to be correct despite the reporting error.

**TABLE 3.4**: Comparison between the mass of measured inlet charge to the engine and the values predicted by GT-POWER for Blend 1 (40°C blend). CR = 10.65 and spark timing = 15 BTDC. San Diego Mechanism used in the below run

| | **Measured** | **Prediction by model when using FluidMixture definition** |
|---|---|---|
| **Air intake (mg/cycle)** | 433.56 | 726.38 |
| **Fuel intake (mg/cycle)** | 361.22 | 44.36 |
| **Total inlet charge (mg/cycle)** | 794.78 | 770.74 |

When Gamma Technologies was approached with this issue, they confirmed it was a technical problem in the software code regarding the reporting of species in such conditions. To overcome this problem, Gamma Technologies recommended to use the 'FluidMixtureCombined' object to define the intake composition to the engine. GT-POWER defines this object as '*A mixture that is combined into a single "pseudo" species*

*with properties that nominally represent the mixture*'. This definition is usually applied to entities such as natural gas which, although has multiple components, but is still treated as a single entity. The newly defined fluid properties are interpolated from the properties of each individual species and their mass fractions. This definition of the syngas allows the software to distinguish between the air and the fuel in the total intake composition and so the trapped masses are correctly reported with almost the same thermal and fluid results as before. FIGURE 3.3 shows the comparison of the measured burned fuel fraction with the results reported by the model using the different fluid definitions. It can be seen that the burned fuel fraction for the FluidMixtureCombined definition is closer to the measured values. The burned fuel fraction predicted for the FluidMixture is very low because of the incorrect reporting of the total fuel entering the engine as explained previously.

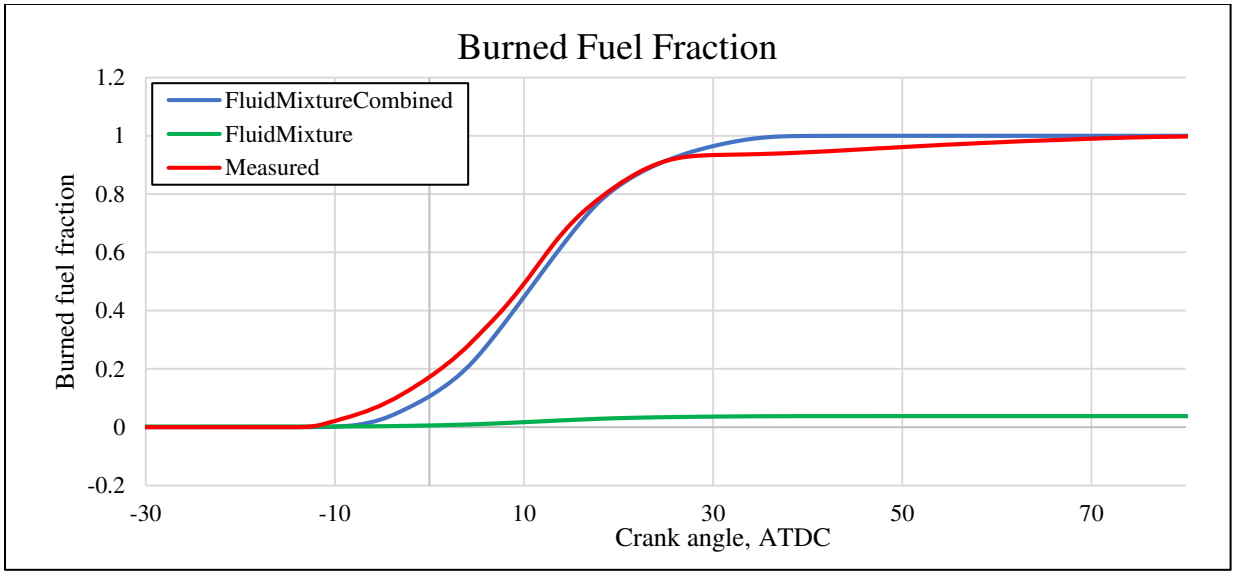


**FIGURE 3.3**: Burned fuel fraction when using different inlet definitions for Blend 1(40°C blend). CR = 10.65, spark timing = 15 BTDC. San Diego mechanism used for the above runs.

But, on further analysis during knock prediction, it was discovered that when using the FluidMixtureCombined definition for the fuel blend, the model could not predict knock phenomenon, even at conditions where knock has a high probability of occurring (i.e., at very high compression ratios). FIGURE 3.4 shows the prediction by the model when subjected to a hypothetical compression ratio of 21 and spark timing of 15 BTDC. The FluidMixture definition predicts knock better than the

FluidMixtureCombined definition. A possible reason for this could be in the definition of the FuidMixtureCombined template. As this template tracks the whole fuel as a single species, the individual reactions of species, such as $H_2$ or CO, may not be properly identified when using the chemical kinetics for knock prediction. This was not the problem when using the FluidMixture definition. It was thus decided to use the FluidMixture definition just for the knock prediction and use the FluidMixtureCombined definition to estimate the performance of the engine when running on the syngas blends. FIGURE 3.5 show the results of the model when both the definitions of the inlet compositions are used. Both the inlet fluid definitions give very similar results to each other when knock is not involved.

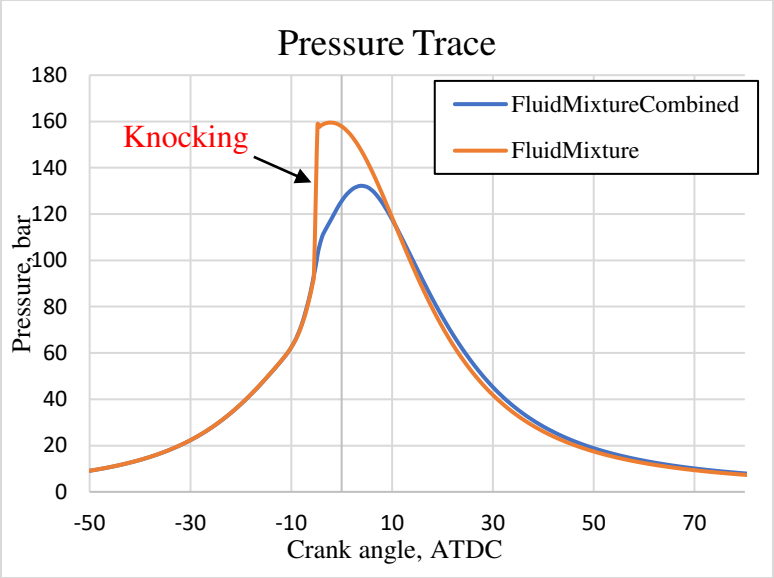


**FIGURE 3.4:** Pressure trace generated by model for Blend 1 (40°C blend) at CR = 21 and spark timing = -15 ATDC. San Diego Mechanism used.

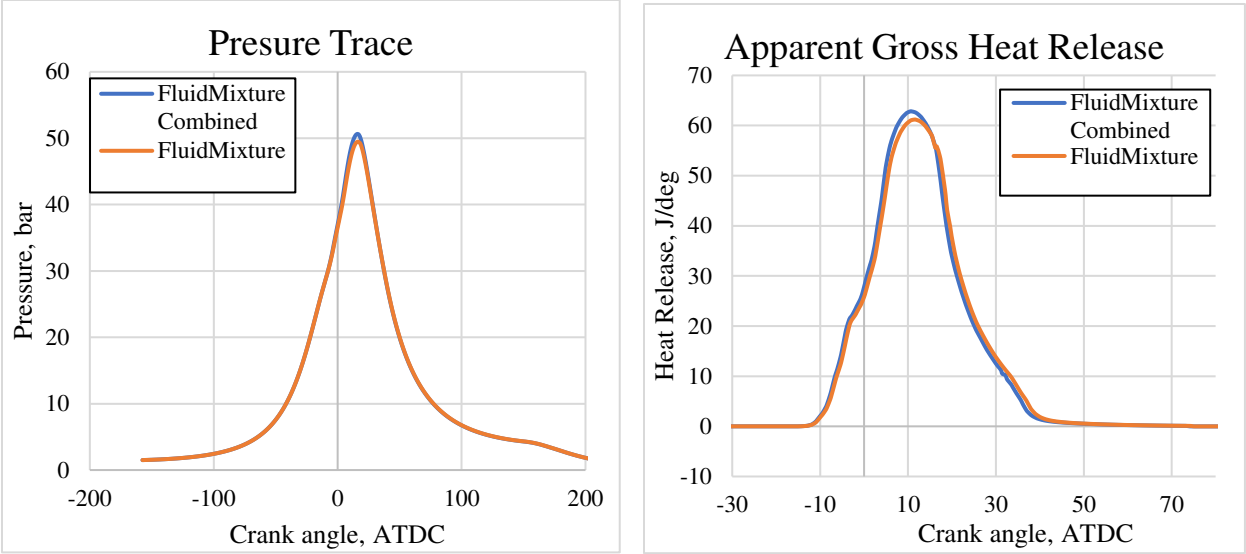


**FIGURE 3.5**: Plots for pressure trace (left) and heat release (right) for Blend 1 (40°C blend) when different inlet definitions are used. San Diego mechanism is used in the model. CR = 10.65, spark timing = -15 ATDC

### *3.2.1.2 Ports and Valves*

The ports of the CFR engine were modelled using the 'Pipe' object in GT-POWER. Details like length of the ports, angle of bend of the ports, diameters of port openings were physically measured from a replica of the cylinder head of the CFR engine shown in FIGURE 3.6.

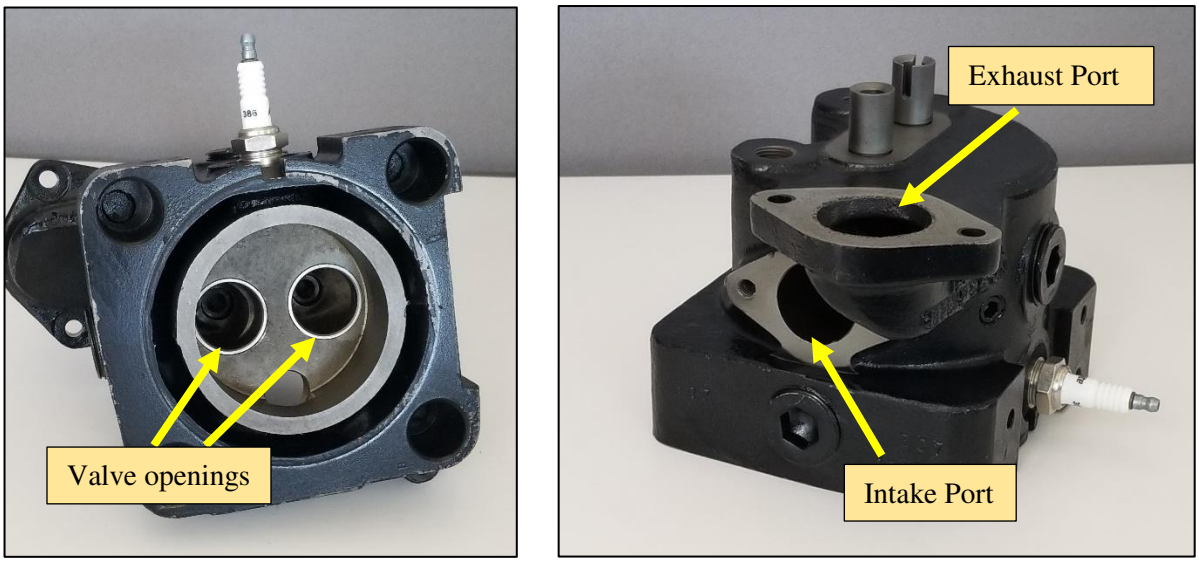


**FIGURE 3.6:** Images of the CFR head replica. Bottom view of the head (left), an isometric view of the head (right)

These details were used to define the pipe component in the model to accurately describe the engine ports' geometry. The cylinder head is made of cast iron [31] and so was used as the material of the port walls. The wall temperature solver of GT-POWER was used in the model to calculate the heat transfer and wall temperatures of the ports during the engine operation.

The 'Valve' connection in GT-POWER was used to model the intake and exhaust valves of the engine. Specifications such as valve timing, lift profile and flow coefficients are important inputs to model the valves correctly. The valve timings and lift profiles of the intake and exhaust valves were obtained from the paper by Choi [19] which used these measured values from the CFR engine for their study and is illustrated in FIGURE 3.7. The flow coefficients of the intake and exhaust valves of the CFR engine were obtained from literature [39] and are shown in FIGURE 3.8.

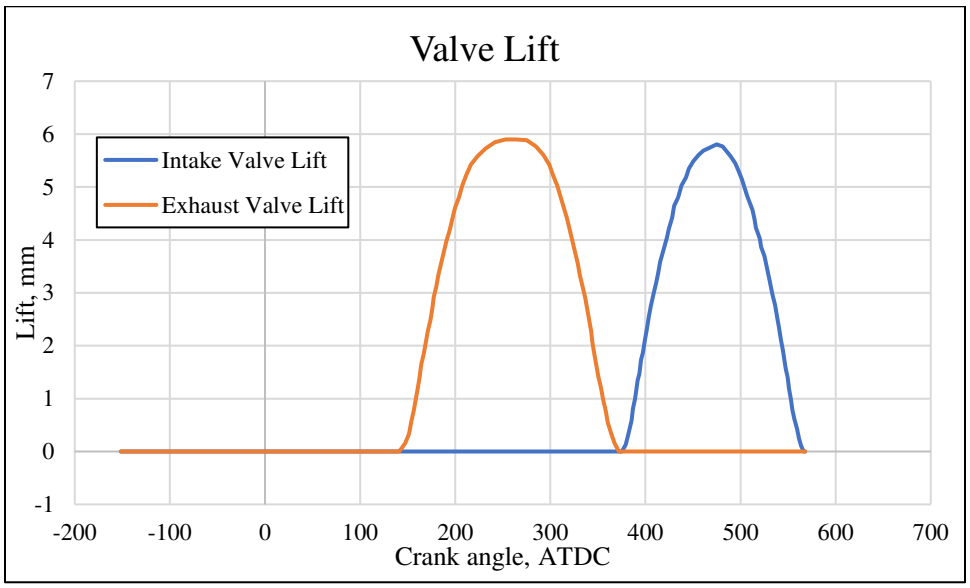


**FIGURE 3.7**: Intake and exhaust valve lifts used in the model

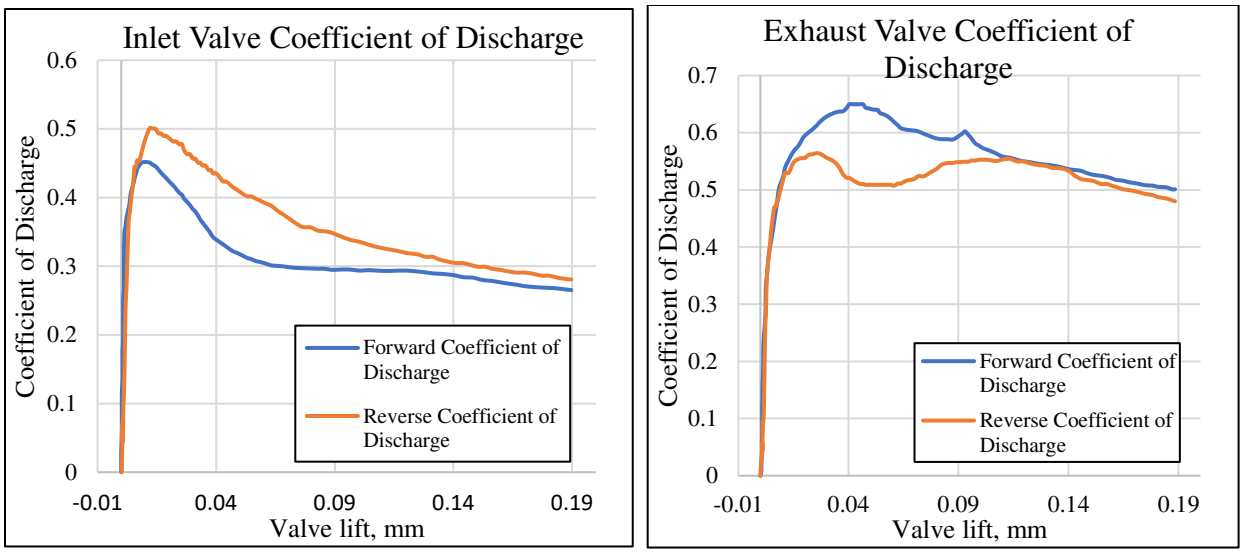


**FIGURE 3.8**: Coefficients of discharge for intake valve (left) and exhaust valve (right) used in the model.

#### *3.2.1.3 Cranktrain and Engine Cylinder*

The 'EngineCrankTrain' object in GT-POWER describes parameters like the cylinder geometry and firing order and is used to model the rigid dynamics and kinematics of typical ICE cranktrain configurations. Other parameters like engine friction and type of engine (2-stroke or 4-stroke) are also defined in this component.

The 'EngCylinder' object is the most important and central element of the modelling process of this study as this represents the part of the engine where the actual combustion of the fuel occurs. This object is used to specify the heat transfer, in-cylinder flow, combustion models and even chemical mechanisms used to describe the combustion process in the cylinder. Important parameters like in-cylinder pressures, fuel burn rates, heat release rates, temperatures inside the combustion chamber, and fluid flow are among the many results which are be obtained from this object and used for critical analysis of the developed model.

### 3.2.2 Three Pressure Analysis modelling

The Three Pressure Analysis (TPA) is primarily used to calculate the burn rate by using the measured pressures from the experiment. This type of calculation is sometimes referred to as 'reverse run' as the measured pressures are the input and the burn rate is the output [13]. In these calculations, the amount of

fuel that is transferred from the unburned to the burned zone is iterated in each time step until the calculated pressures match the measured pressures. There are no simplifying assumptions made during these reverse runs and include the full thermodynamics and chemistry that are used in a conventional forward run.

For the TPA, as the name suggests, three measured pressures are required as the inputs to the model: intake pressure, in-cylinder pressure, and exhaust pressure. The simulation methodology used in the TPA runs, as explained in the GT-POWER manual [13], is explained below.

1. *For cycle 1, a dummy burn rate is used, and no pressure analysis is performed*
2. *For cycle 2 and beyond, the forward run simulation will "pause" at the start of each cycle and calculate the apparent burn rate using the trapped conditions in the cylinder at that point (typically IVC) along with the measured pressure profile.*
3. *The forward simulation run continues and the apparent burn rate calculated in the previous step is imposed during the cycle*
4. *Cycles repeat until steady state convergence is reached.*

The main advantage of this approach is that all the cylinder trapped quantities, like residual fraction and trapped mass, are predicted by the simulation. This feature was utilized in many previous studies, as mentioned in the literature review, to get the cylinder conditions at IVC and used as boundary conditions in subsequent models. The disadvantage of this approach is that multiple data points are required to accurately describe the engine operation and that the calculations could get slower since the cycles need to run till convergence. However, the TPA runs are much faster and require lesser computation power when compared other CAE methods such as 3-D CFD modelling.

In the current study, measurements from the engine were taken at different operating points of spark timings and compression ratios. The measured pressures and temperatures at the intake and exhaust of the engine were used in the end-environment boundary conditions. The in-cylinder pressures at each of the corresponding operating points were also used as the input to the TPA model. Examples of these pressures

are shown in FIGURE 3.9 and 3.10. Each of the measured pressures and temperatures was obtained in a crank angle resolved manner for a complete cycle of the engine and was collected for over 500 or 1000 consecutive engine cycles. The data from each operating point was averaged and used in the TPA to get an average burn rate for that condition. Although GT-POWER has a feature to use the data from all the individually measured cycles for an operating point, the averaged input method was chosen to reduce the effect of possible errors or noise gathered in random cycles throughout the experiment. The averaged method is also computationally faster and was thus preferred. Additional inputs to the model include composition of the fuel blend input to the model, which allows the software to calculate the heat release and burn rates for the analysis.

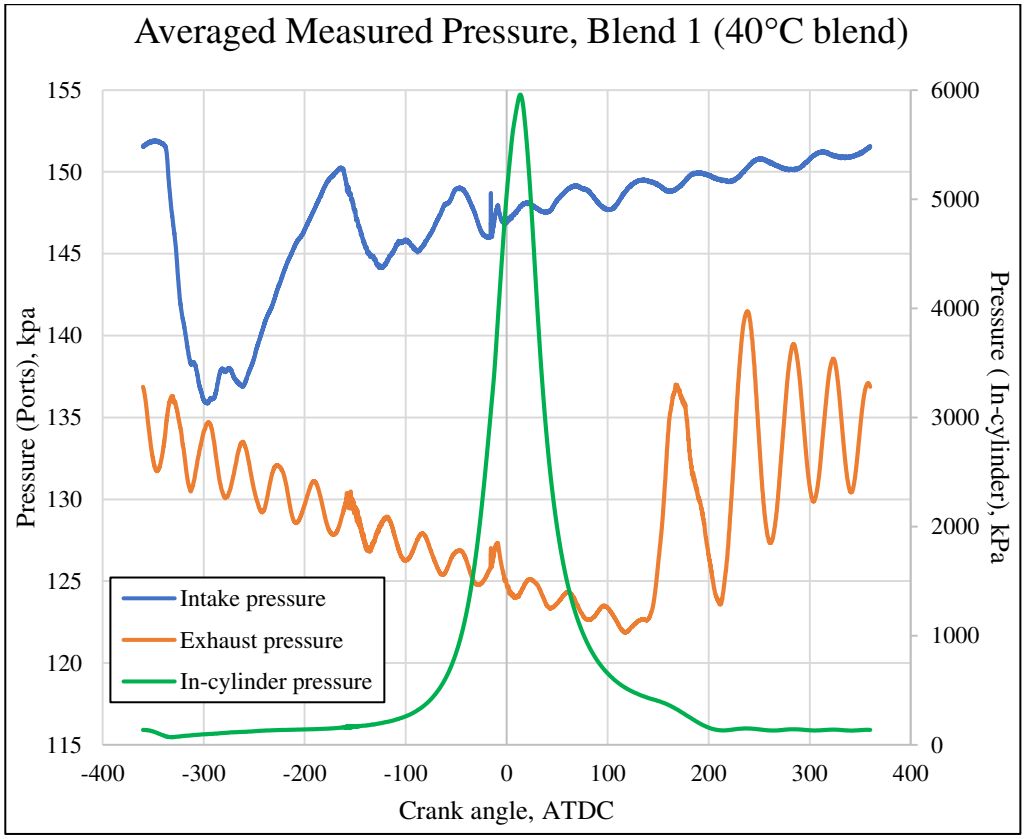


**FIGURE 3.9:** Average measured pressure traces for Blend 1 (2.45 mol% $H_2O$) for a CR = 10.65 and spark timing of -15 ATDC

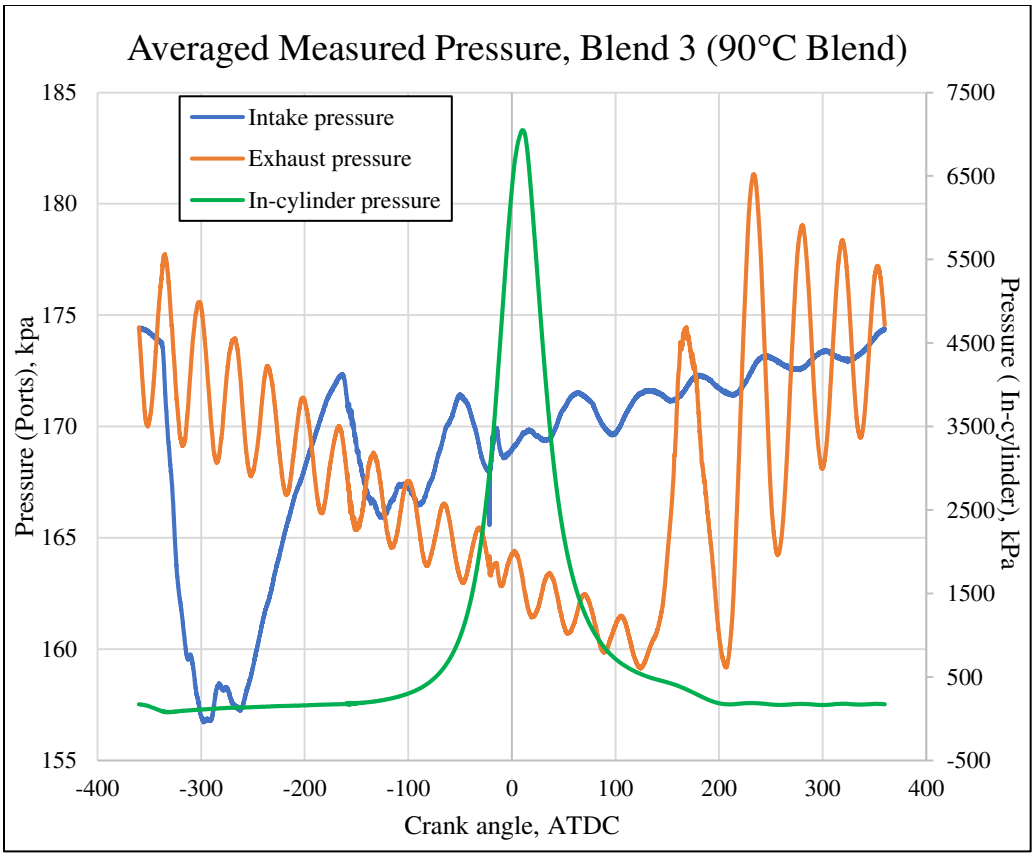


**FIGURE 3.10:** Average measured pressure traces for Blend 3 (23.3 mol% $H_2O$) for a CR = 12.14 and spark timing of -21 ATDC

The results of TPA simulation does not always match the measured data in the very first iteration when just using the default model multipliers. To improve the TPA results, certain parameters or multipliers in the model can be adjusted. In these kinds of simulations, the heat transfer models are usually the biggest sources of uncertainty. So, parameters related to heat transfer in the engine such as the in-cylinder convection coefficient and the intake and exhaust port heat transfer multipliers can be adjusted within a reasonable window to get results that better match the measured data. Detailed equations used by GT-POWER for the heat transfer coefficients and multipliers are shown in Appendix 1 [40]. In this study, in addition to the heat transfer model multipliers, the flow area multipliers of the intake and exhaust valve were also slightly changed within reasonable limits to match the trapped masses. The burn rate results from TPA results can be accurate only if the model replicates the engine data to a good degree. In this study the in-cylinder pressure trace and the trapped mass per cycle values were considered for determining how good the results

of the TPA were. The goal was to have a maximum error of 5% between the measured data and simulated results. When comparing the pressure trace between the TPA and the measured data, only the in-cylinder pressures during the compression and expansion stroke was considered. By understanding how changes in the heat transfer and flow area multipliers have on the results, multiple runs of the TPA model were performed to get the best match to the measured data.

### 3.2.3 Predictive Combustion Model

Up until the completion of the TPA model, no combustion model was used in this study's process. The TPA modelling does not necessarily require any definition of any combustion object in the cylinder. GT-POWER determines the combustion burn rate at the measured operating points based on the input parameters supplied, such as the pressures and composition of the inlet fuel and uses the information present in the software's databases. However, the aim of this study is to develop a predictive model that can determine the combustion burn rate at any operating point and not just match results from measured data. For developing a predictive combustion model, an attribute describing how the fuel burns (e.g., flame speeds, ignition delay, LHVs etc.,) should be included in the analysis. In this thesis, the laminar flame speed of the fuel blends was chosen as that attribute. As mentioned earlier in the literature review, documentation on flame speeds for custom syngas mixtures is very sparse. To solve this issue, the software CHEMKIN was used to calculate the flame speeds of the fuel blends used in the current study. CHEMKIN has been used in previous studies to validate flame speeds for fuels such as biofuels and different types of syngas-type mixtures. Details on the role of CHEMKIN in flame speed modelling is explained later. The results from the flame speed modelling are used in the development of the combustion model in GT-POWER.

Once the combustion model is be developed, it must be calibrated to be able to output predictive results without any change in the model inputs. GT-POWER offers a tool named "Measured + Predicted Converter" (M+P Converter) that allows the combustion model to be calibrated once developed. Once the TPA model is adjusted to satisfactory levels, the M+P Converter is used to set up the M+P Analysis model. This model allows the selection of a combustion object template to be used in the overall engine model. In

the current study the template "EngCylCombSITurb" in GT-POWER is used to model the combustion object which is later calibrated.

The EngCylCombSITurb template, often abbreviated as 'SITurb', is used in the EngCylinder object. The template predicts the burn rate for homogenous charge spark-ignition engines and requires inputs that are used to model the combustion inside the cylinder. Examples of the inputs include positions of the spark plug and valves, geometry of the cylinder, cylinder heat transfer model, fuel properties, and flow properties inside the cylinder. The SITurb models the combustion of the fuel by accounting for the flame speeds, both laminar and turbulent, of the burning fuel. Details of the flame speeds and burn rate calculations are discussed in the below sections.

#### *3.2.3.1 Laminar Flame Speeds*

To calculate the laminar flame speeds of the fuel, GT-POWER uses the following equation:

$$S_L = (B_m + B_\emptyset\ (\emptyset - \emptyset_m)^2)\ \left(\frac{T_u}{T_{ref}}\right)^\alpha\ \left(\frac{\rho}{\rho_{ref}}\right)^\beta\ f(Dilution) \quad \text{…Eqn. 3.5}$$

where, $S_L$ is the laminar flame speed, $B_m$ is the maximum laminar flame speed propagating through the fuel/air mixture at a pressure of 1 atm and a temperature of 300K, $B_\emptyset$ is the laminar speed roll-off value used to describe the decay profile of the flame speed from its maximum value, $\emptyset$ is the in-cylinder equivalence ratio, $\emptyset_m$ is the equivalence ratio at maximum laminar speed, $T_u$ is the temperature of the unburned gas, $T_{ref}$ is the reference temperature of 300 K, $\rho$ denotes pressure and $\rho_{ref}$ is the reference pressure of 1 atm. $\alpha$ and $\beta$ represent the temperature and pressure exponents respectively. *f(Dilution)* represents the dilution effect and is defined using the following correlation developed by GT:

$$f(Dilution) = 1 - 0.75 * DEM\ (1 - (1 - 0.75 * DEM * Dilution)^7) \quad \text{…Eqn. 3.6}$$

where, *Dilution* is the mass fraction of the residuals in the unburned zone and *DEM* stands for Dilution Effect Multiplier.

For conventional fuels, like gasoline or methane, the values of the term coefficients are already present in the software's databases. These coefficients have been obtained from existing literature about experiments

using those fuels. However, for the custom syngas mixtures in this study, such literature is not available. To overcome the deficiency, the values of the term coefficients were calculated using a simple numerical approximation. To get the values of term coefficients, a simplified form of eqn. 3.5, shown in eqn. 3.7, available in Heywood, [41] was used and fit to laminar flame speeds calculated with Chemkin:

$$S_L = (B_m + B_{\emptyset}\ (\emptyset - \emptyset_m)^2)\ \left(\frac{Tu}{T_{ref}}\right)^{\alpha}\ \left(\frac{\rho}{\rho_{ref}}\right)^{\alpha} \quad \text{…Eqn. 3.7}$$

The definition of the terms for eqn. 3.7 are the same as for eqn. 3.5. Eqn. 3.7 does not include the dilution effect correlation developed by GT. From the definition available in the help section of GT-POWER, *f(Dilution)* is used to scale the effect of dilution in the form of residuals and exhaust gas recirculation (EGR) on the laminar flame speeds and thus is less relevant to this study as we are not operating with EGR. The *DEM* in eqn. 3.6 is later assigned a value during the calibration process and the reasoning is explained in the corresponding section. Taking these factors into consideration, the dilution effect in eqn 3.5 was neglected in the flame speed calculations and eqn. 3.7 was used instead to determine the values of the term coefficients.

#### *3.2.3.2 Turbulent flame speed and burn rates*

A two-zone modelling of combustion requires analysis of the fuel being burnt and the unburnt fuel in the combustion chamber. The analysis needs to be done simultaneously for each time step. For the burning fuel parameters such as burn rate of the fuel, rate at which the unburnt fuel enters the flame front, energy given off during combustion, heat transfer to the surroundings etc., are few examples which must be taken into account. The turbulence and velocities of the unburnt fuel affects the way the flame front propagates and is closely linked with the parameters of the burning fuel mentioned earlier. Also, based on the conditions of the combustion chamber and the properties of the unburnt fuel (by using chemical mechanisms), knocking in the engine can be determined. Thus, turbulent flame speeds and burn rates are important modelling parameters for a two-zone combustion model. FIGURE 3.11 is an illustration of how a flame propagates in the combustion chamber of an engine and highlights some of the key considerations in two-zone modelling.

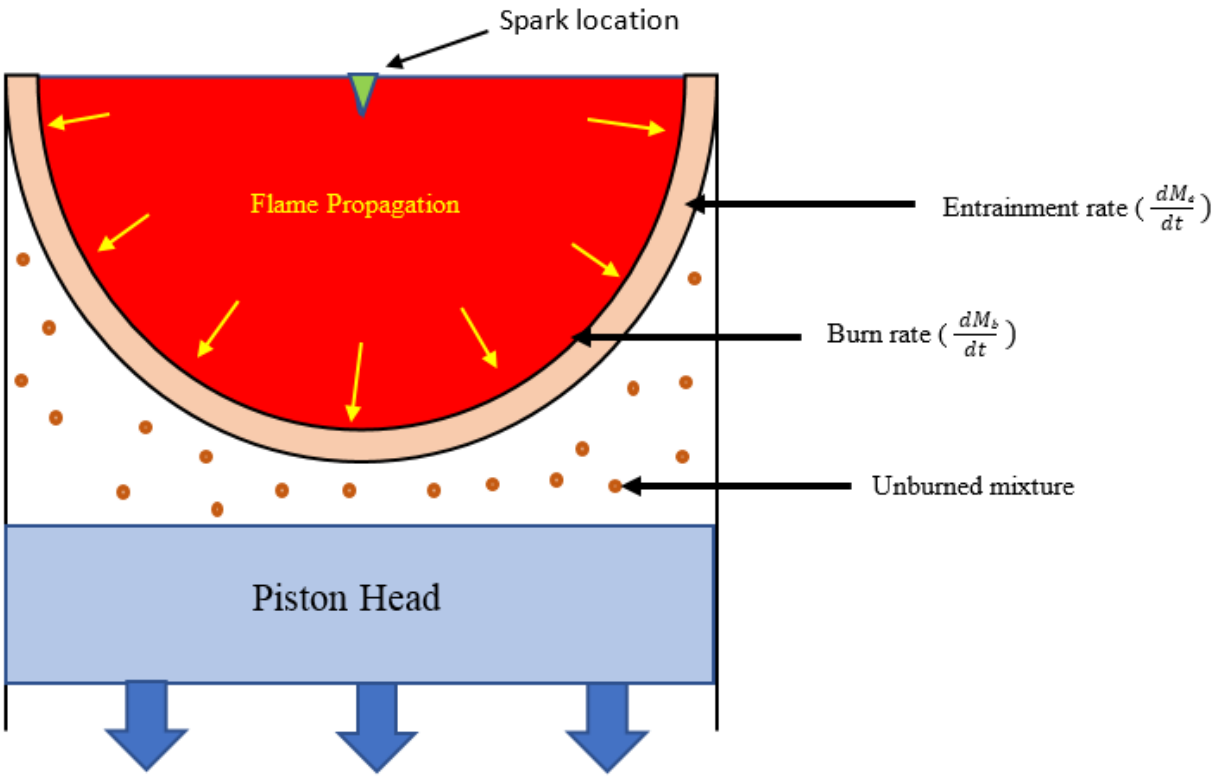


**FIGURE 3.11**: Illustration of flame propagation inside the engine

The rate of unburned fuel-air mixture entrained into the flame front is proportional to the sum of the laminar and turbulent flame speeds [13]. This is calculated using the eqn 3.8. The burn rate is proportional to the mass of unburned mixture behind the flame front divided by a time constant, $\tau$, and is shown by the eqn. 3.9.

$$\frac{dM_e}{dt} = \rho_u A_e (S_T + S_L) \quad \text{…Eqn. 3.8}$$

$$\frac{dM_b}{dt} = \frac{(M_e - M_b)}{\tau} \quad \text{… Eqn. 3.9}$$

where, $M_e$ is the entrained mass, $M_b$ is the burned mass, $\rho_u$ represents the unburned density, $A_e$ is the surface area at flame front, $S_T$ is the turbulent flame speed and $\tau$ is the time constant.

The SITurb model uses the in-cylinder flow reference object 'EngCylFlow' to collect information on the turbulent intensity and length scale. The turbulence and the turbulence flame speeds are characterized by three multipliers: Flame Kernel Growth multiplier, Turbulent Flame Speed multiplier, and Taylor Length

Scale multiplier. The Flame Kernel Growth multiplier is used to scale the calculated value of the growth of the flame kernel and influences the self-sustainability of the initiated flame once the spark ignites the fuel. Larger values increases the initial flame growth, advancing the transition from laminar to turbulent combustion. The Turbulent Flame Speed multiplier is used to scale the calculated turbulent flame speed. Larger numbers increase the speed of combustion and so influences the overall duration of the combustion. The Taylor Length Scale multiplier is used to scale the 'Taylor microscale' of turbulence. The Taylor Length Scale represents a characteristic length associated with the ratio of dissipation of turbulent kinetic energy and turbulent kinetic energy itself [42]. The multiplier thus modifies the time constant of combustion of the fuel/air mixture entrainment into the flame zone by changing the thickness of the plume. The following equations are used to calculate the turbulent flame speeds in GT-POWER [13]:

$$\tau = \frac{\lambda}{S_L} \quad \text{…Eqn. 3.10}$$

$$S_T = C_{TFS}\, u' \left(1 - \frac{1}{1 + C_{FKG}\left(\frac{R_f}{L_i}\right)^2}\right) \quad \text{… Eqn. 3.11}$$

$$\lambda = \frac{C_{TLS} L_i}{\sqrt{Re_t}} \quad \text{… Eqn. 3.12}$$

$$Re_t = \frac{\rho_u\, u' L_i}{\mu_u} \quad \text{… Eqn. 3.13}$$

$C_{TFS}$ = Turbulent flame speed mutiplier
$C_{TLS}$ = Taylor length scale multiplier
$S_T$ = Turbulent flame speed
$u'$ = Turbulent intensity
$R_f$ = Flame radius
$\mu_u$ = Unburned zone dynamic viscosity
$C_{FKG}$ = Flame kernel growth multiplier
$\lambda$ = Taylor microscale length
$L_i$ = Integral length scale
$Re_t$ = Turbulent Reynolds number
$\rho_u$ = Unburned density

## 3.3 CHEMKIN Modelling

Modelling the flame speeds for the syngas fuels using CHEMKIN gives values of the constituent terms for the laminar flame speed equation of eqn. 3.7. In this thesis, first the laminar flame speeds for the syngas blends were estimated at different temperatures and pressures using CHEMKIN. Three different chemical mechanisms were selected for use in the software: the San Diego mechanism [43], the GRI-mechanism [44], and the hydrogen syngas mechanism of NUI-Galway [45]. The San Diego mechanism contains 58 species and 268 reactions [43]. The chemistry used is designed to focus on conditions relevant to flames, high temperature ignition and detonations. The GRI mechanism is an optimized mechanism designed to model natural gas combustion, including NO formation and re-burn chemistry. Although initially developed for methane combustion it is widely used in syngas-related studies. It contains 325 reactions and 53 species [44]. The hydrogen syngas mechanism of NUI-Galway was developed to model syngas with hydrogen and carbon monoxide as the main combustive entities in a syngas mixture. It consists of 15 species and 48 reactions [45].

The NUIG-syngas mechanism does not have methane defined in its species list and so has no hydrocarbon fuel reactions. As the methane composition is very minor in the blends (<1% mole fraction) it was decided to overlook this absence of methane in the mechanism and decide if the mechanism is appropriate enough to model the syngas based on the results obtained. So, in cases where the NUIG-syngas mechanism was used, the inlet composition of the gases in the GT-POWER model was modified accordingly to account for the absence of methane in the mixture. This was done even during the TPA simulations. The mechanism also included an excited species of OH named as OH* which caused a minor problem in GT-POWER. The software contains 13 standard products of combustion of which OH is a part. However, GT-POWER could not distinguish the OH* in the mechanism and would erroneously map the OH and OH* to the same burned species during the runs. Upon approaching GT-support, they suggested to commenting out the reactions with OH* and removing the OH* from the species list. The suggested change to the mechanism was made and run in CHEMKIN to compare the flame speeds and ignition delays obtained with and without the OH*

in the chemical mechanism. There was not much change in the flame speeds between the original and modified mechanism. The comparison of the flame speeds for the two mechanisms for both the blends is shown in FIGURE A2.1 and FIGURE A2.2 in Appendix 2. Also, the ignition delays for both the cases were almost identical for the range of temperatures and pressures CHEMKIN was run on. This ensured that the modelling of the syngas combustion would not change significantly with the OH* species removed from the mechanism. After the modification, the NUIG-syngas mechanism consisted of 14 species and 37 reactions. Another mechanism, AramcoMech 3.0 (581 species and 3237 reactions), also from NUI-Galway [46], was attempted to be used for the chemical kinetics in this study. However, the bigger size of this mechanism caused memory related errors in GT-POWER while importing the mechanism file during the simulations. Due to this issue, the mechanism was dropped from the analysis and the study continued with the 3 previously mentioned mechanisms. The mechanisms chosen were also included in the group of mechanism selected in a previous work by Olm et. al, 2015 [47] to compare their performance to model syngas combustion.

The flame speeds were calculated over a range of temperatures and pressures using the different chemical mechanisms. The temperatures ranged from 300 K to 1000 K in increments of 10 K and the pressures ranged from 1 atm. to 51 atm. in increments of 5 atm. The values of flame speeds derived from eqn. 3.7 was then fit to the values of the flame speeds obtained from CHEMKIN at the corresponding pressures and temperatures. The fit was obtained by adjusting the coefficients $B_{\emptyset}$, $\alpha$, and $\beta$. The term $B_m$ and $\Phi_m$ was calculated by finding the maximum flame speed at a pressure of 1 atm. and 303 K over a range of equivalence ratios using CHEMKIN. Since the syngas was to be burnt at stoichiometric conditions, the value of $\Phi$ was set to 1. The solver present in Microsoft Excel was used to then find values of $B_{\Phi}$, $\alpha$, and $\beta$ to get the best possible fit by minimizing the sum of squared errors (SSEs) between the flame speeds predicted from CHEMKIN and the flame speeds calculated from eqn. 3.7. FIGURE 3.12 - 3.17 show examples illustrating the fit of the flame speeds for Blend 1 and Blend 3 when using the different mechanisms.

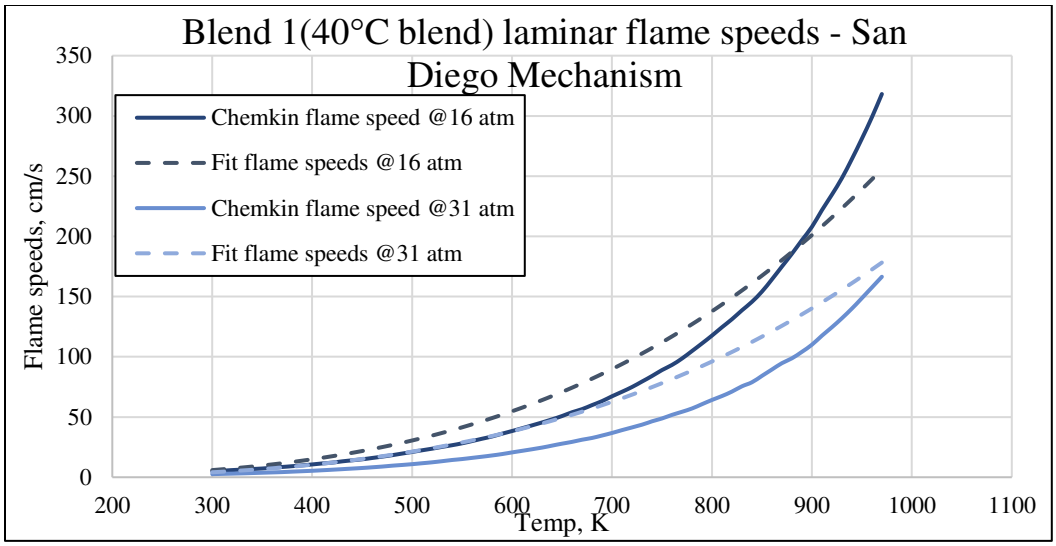


**FIGURE 3.12**: Plots of the CHEMKIN and calculated flame speed of Blend 1(2.45 mol% $H_2O$) when using the San Diego mechanism

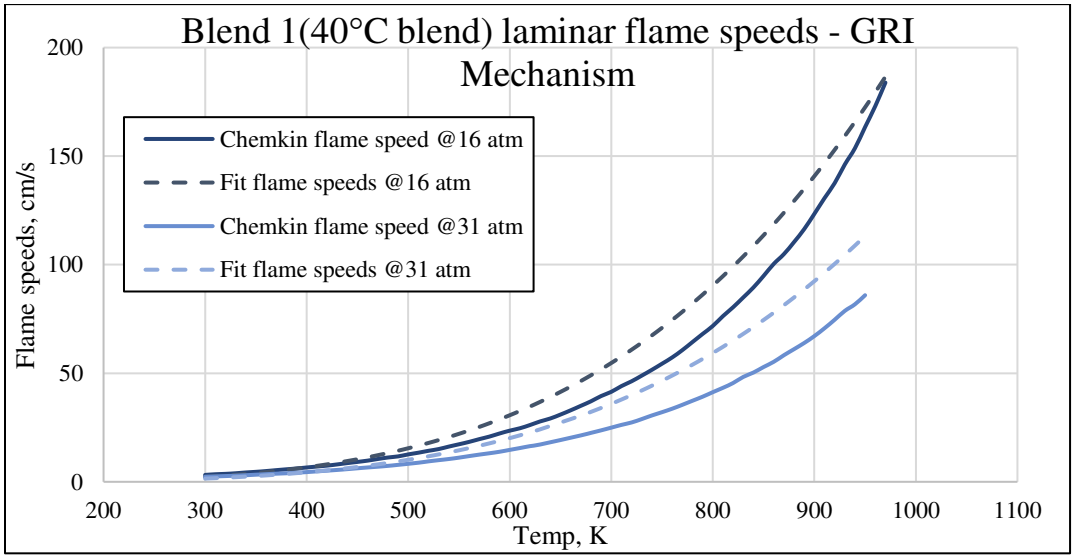


**FIGURE 3.13**: Plots of the CHEMKIN and calculated flame speed of Blend 1 (2.45 mol% $H_2O$) when using the GRI mechanism

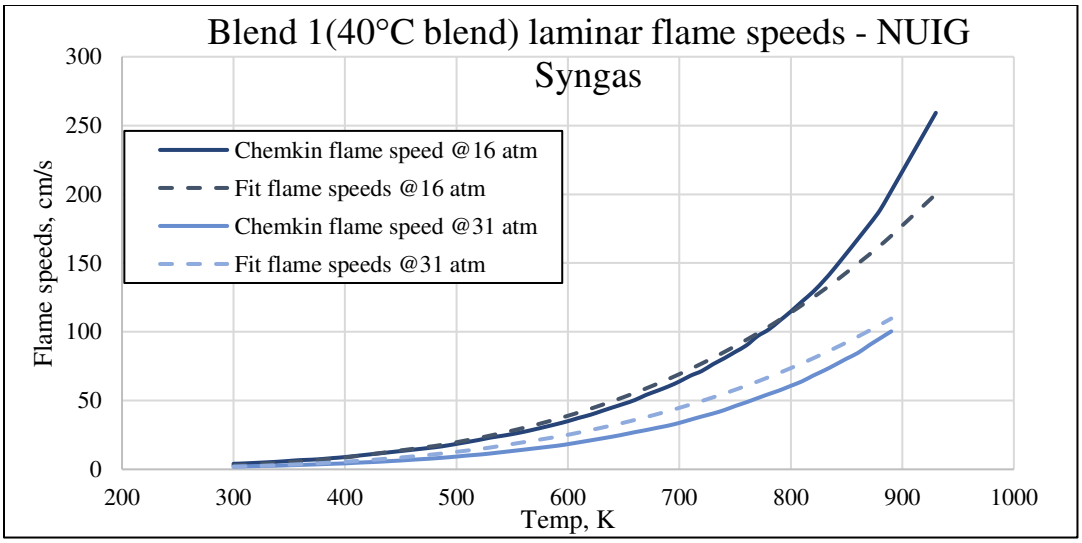


**FIGURE 3.14**: Plots of the CHEMKIN and calculated flame speed of Blend 1 (2.45 mol% $H_2O$) when using the NUIG-Syngas mechanism

**TABLE 3.5:** Laminar flame speed parameters for Blend 1 (2.45 mol% $H_2O$) when using San Diego mechanism, GRI mechanism, and NUIG-Syngas mechanism

| | **San Diego** | **GRI** | **NUIG-Syngas** |
|---|---|---|---|
| Maximum Laminar Speed *($B_m$)* | 35.76532 | 31.71927 | 45.96168 |
| Laminar Speed Roll-off Value *($B_\phi$)* | -200 | -200 | -133.24 |
| Equivalence Ratio at Maximum Speed *($\phi_m$)* | 1.2 | 1.3 | 1.45 |
| Temperature Exponent *($\alpha$)* | 3.207215 | 3.760008 | 3.734535 |
| Pressure Exponent ($\beta$) | -0.5453 | -0.6366 | -0.66104 |
| Dilution Effect Multiplier (DEM) | 0.2 | 0.2 | 0.2 |

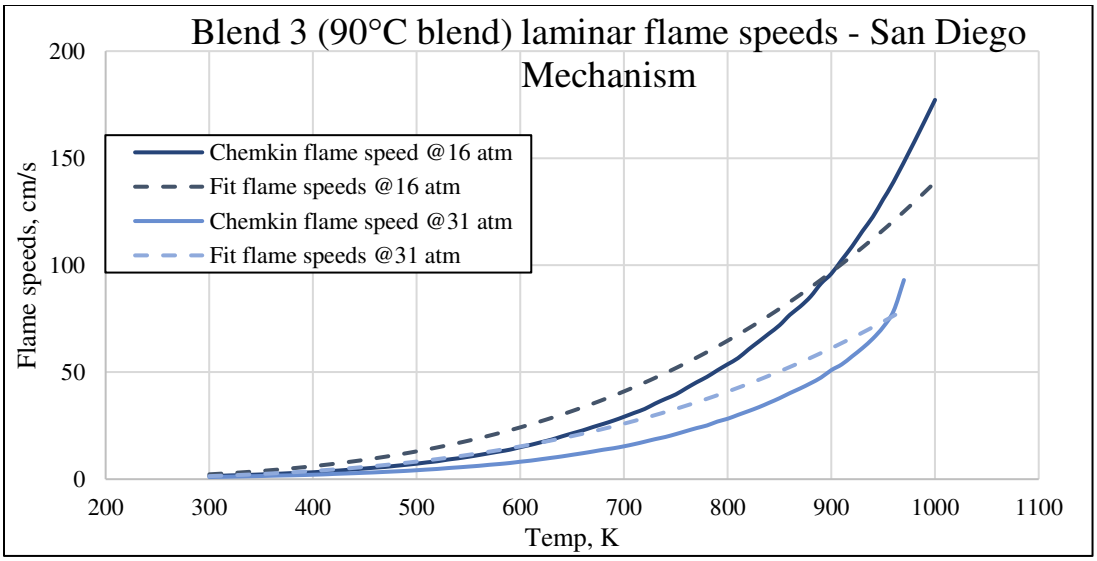


**FIGURE 3.15**: Plots of the CHEMKIN and calculated flame speed of Blend 3 (23.3 mol% $H_2O$) when using the San Diego mechanism

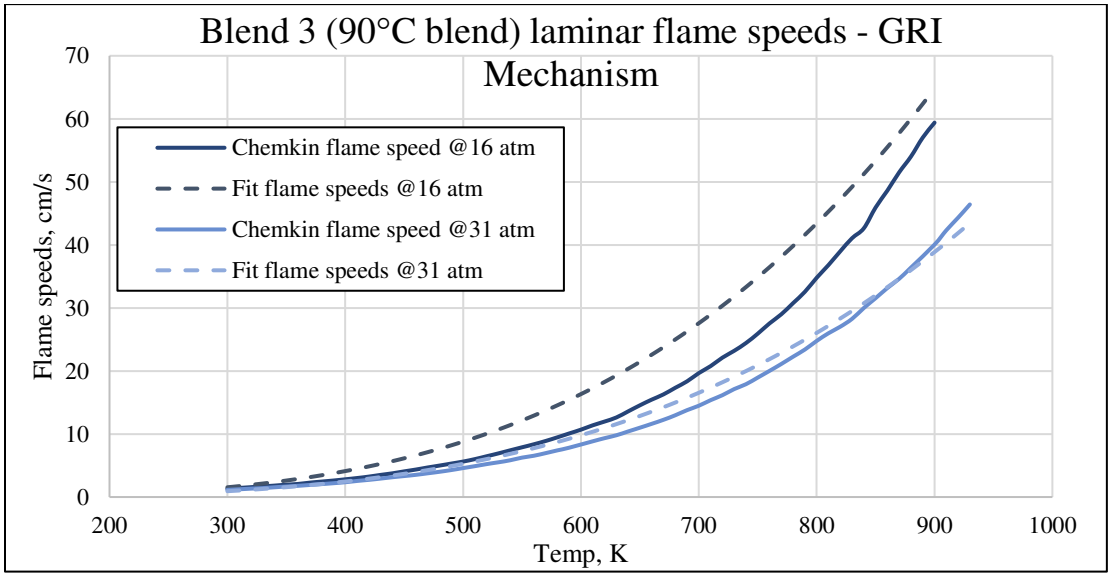


**FIGURE 3.16**: Plots of the CHEMKIN and calculated flame speed of Blend 3 (23.3 mol% $H_2O$) when using the GRI mechanism

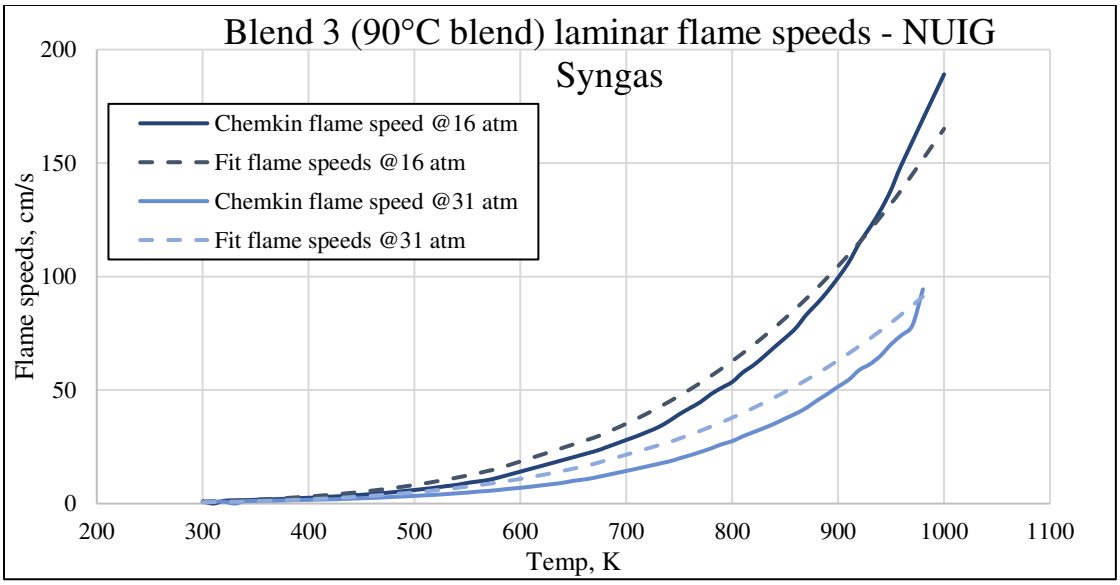


**FIGURE 3.17**: Plots of the CHEMKIN and calculated flame speed of Blend 3 (23.3 mol% $H_2O$) when using the NUIG-Syngas mechanism

**TABLE 3.6**: Laminar flame speed parameters for Blend 3 (23.3 mol% $H_2O$) when using San Diego mechanism, GRI mechanism, and NUIG-Syngas mechanism

| | **San Diego** | **GRI** | **NUIG-Syngas** |
|---|---|---|---|
| Maximum Laminar Speed ($B_m$) | 18.00344 | 14.144 | 22.59418 |
| Laminar Speed Roll-off Value ($B_\phi$) | -200 | -200 | -164.395029 |
| Equivalence Ratio at Maximum Speed ($\phi_m$) | 1.1 | 1.05 | 1.3 |
| Temperature Exponent ($\alpha$) | 3.416738 | 3.398477 | 4.332728 |
| Pressure Exponent (β) | -0.692437 | -0.772565 | -0.764837 |
| Dilution Effect Multiplier (DEM) | 0.2 | 0.2 | 0.2 |

The flame speeds of the syngas blends were also compared with those of methane using the GRI and the San Diego mechanism. The comparison was done for at a pressure of 1 atm. FIGURE 3.18 shows the comparison of the methane flame speeds with the syngas blends when using the corresponding chemical mechanisms. The comparison gives an estimate of how reactive the syngas blends were in comparison to a standard fuel, i.e., methane. The comparison shows that the syngas blends, including Blend 3 (which has the highest water content of 23.29 mol percent) have higher flame speeds than methane at higher temperature ranges like those usually experienced during the combustion in an ICE.

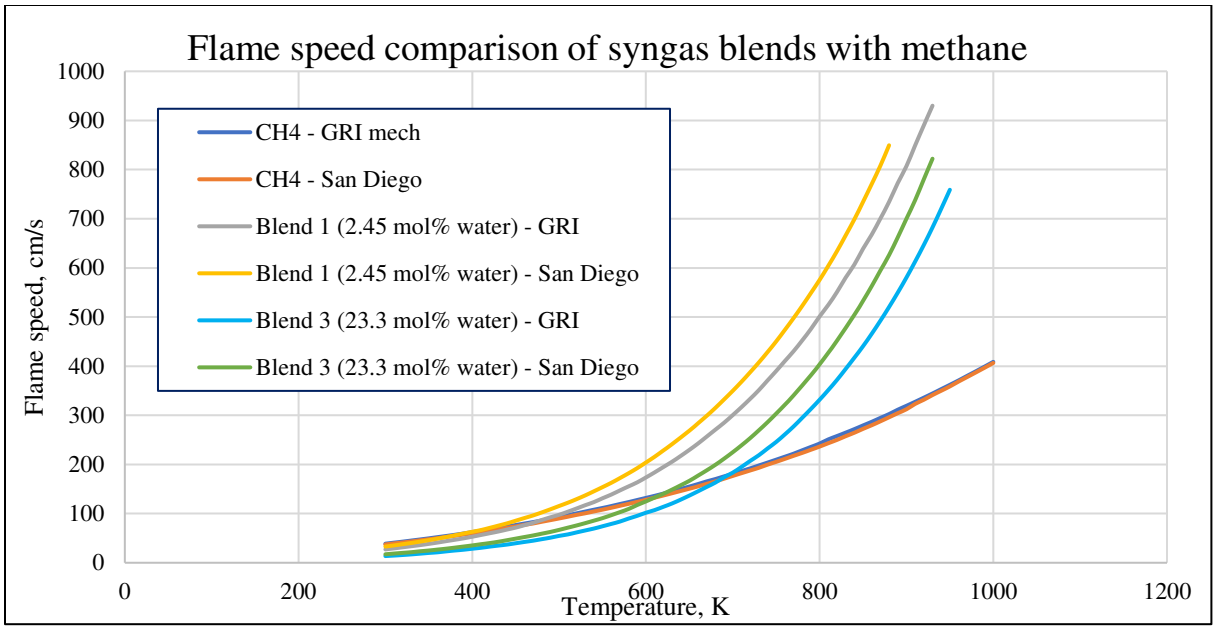


**FIGURE 3.18:** Comparison of flame speeds of methane with the syngas blends using GRI and San Diego mechanisms at 1 atm. pressure.

In addition to the flame speeds, a knock model is also setup in the SITurb template by inputting the chemical mechanism along with the thermodynamic data file to be used in the model. The chemical mechanism will be used in each cycle of the simulation in the model to predict if a given operating point is prone to knocking or not. In this study the mechanisms used to determine the laminar flame speed, i.e., the San Diego mechanism, the GRI mechanism, and the hydrogen syngas mechanism of NUIG were also used for the knock analysis. GT-Power uses a different approach to calculate the KI in the engine than the method used in the experiment. The FFT method used in the experiment is explained in section 2.1 and an example is shown in FIGURE 2.3. The software uses the empirical formula shown in eqn. 3.14 to calculate the KI.

$$KI = 10000 * M * u * \frac{V_{TDC}}{V} * exp\left(\frac{-6000}{T}\right) \max(0,1-(1-\emptyset)^2) * \frac{I_{ave}}{I_{K\text{-}ref} * I_{K\text{-}corr}} \quad \text{…Eqn. 3.14}$$

where,

$KI$ = knock index
$M$ = knock index multiplier
$u$ = percentage of unburned mass at knock initiation
$V_{TDC}$ = cylinder volume at TDC
$V$ =cylinder volume at knock initiation
$T$ = Bulk instantaneous unburned gas temperature at knock initiation
$\Phi$ = equivalence ratio of unburned zone at knock initiation
$I_{ave}$ = induction time integral, averaged over all end zones at knock initiation
$I_{K\text{-}ref}$ = reference induction time integral
$I_{K\text{-}corr}$ = induction time integral correlation factor

Once all the components of the combustion model are defined in the M+P model, the calibration step is then performed. The goal of the calibration is to obtain a single set of model multipliers that will provide the best possible match to a variety of operating points. To match the predicted and measured burn rates averaged over all data points, GT-POWER recommends finding the best values of four main SITurb attributes: Flame Kernel Growth multiplier, Turbulent Flame Speed multiplier, Taylor Length Scale multiplier, and the Dilution Exponent Multiplier (DEM). This study follows the calibration recommendation but with a slight modification. The value of the DEM was fixed at the least possible value of 0.2. This was done to account for the higher dilution inherently present in the syngas being used. GT-POWER tracks the syngas mixture as a single species and the properties of this species is interpolated from the individual constituents and their mass fractions in the mixture. The significant percentage of non-combustive gases could appear as unburnt gas residuals in the engine during the combustion of the syngas. This could increase the effect of dilution in the laminar flame speed calculations by the software when using eqn. 3.5, thus reducing the overall laminar speed for the fuel. To avoid incorrect predictions from the model due to the reduced flame speeds, the *DEM* was reduced to the minimum possible value of 0.2 in the software.

To get good predictive results, many operating points must be used during the calibration process. In this study, 19 operating points were used for Blend 1 and 16 data points for Blend 3 during the TPA and the combustion model calibration. Three operating points were withheld for validation of the models for both the blends. The M+P Analysis model in GT-Power performs a closed volume pressure analysis during the calibration. The M+P converter initializes the calibration model with values from the TPA simulations performed previously. The turbulent flame multipliers were initially given default values of '1' in the combustion model. Using the Integrated Design Optimizer (IDO) present in GT-POWER, the values of the three multipliers in SITurb are optimized to match the predicted burn rates from the combustion model with the averaged burn rates measured from the experiments. As recommended in the manual [13], the optimized

multipliers are limited to values between 0.5 and 3. The IDO manipulates the values of the multipliers within this range to match the averaged burn rates predicted by the TPA. After completion of the optimization process by the IDO, the values of the new calibrated multipliers are used in the combustion model to get predictive results. The model is then validated against the 3 operating points withheld to check the predictive quality of the model. FIGURE 3.19 illustrates this process.

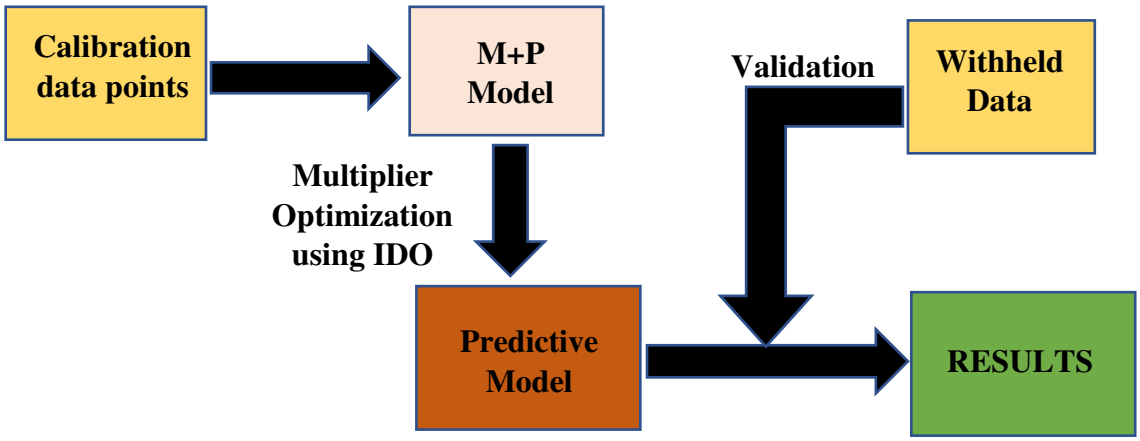


**FIGURE 3.19**: Calibration and validation process for the predictive model

# Chapter 4: Results and Discussion

The experimentation on the CFR engine with the syngas mixtures and the consolidation of the results were performed by additional graduate students working on the project. The data obtained from those tests were used for modelling the engine and validating the model developed in this study, and thus will be presented here to evaluate model fidelity. As mentioned earlier, Blend 1 and Blend 3 were the focus of the current study. Blend 1 would be the composition at the lowest temperature that is attainable (i.e., 40°C) using the intercooler available, and thus the syngas blend which would have the highest heating value (due lowest water content and higher $H_2$ concentration) of the available mixtures. Blend 3 was studied to understand how a fuel having a lower heating value, but potentially more knock resistance, would behave upon combustion in the CFR engine.

## 4.1 TPA Results

Using the intake pressure, in-cylinder pressure and the exhaust pressure of the engine, the TPA was performed in GT-POWER. Since the TPA does not require any combustion modeling, no chemical mechanism file was input during this process. This can be seen in FIGURE 3.1. The TPA results were the same for each blend when the inlet composition was the same. These results can be used for any chemical mechanism later in developing the combustion model as long as the inlet composition is the same. But since the NUIG-syngas mechanism had no methane in it, the TPA runs intended to support this mechanism had the inlet composition modified to account for no methane. These TPA results were however, marginally different than the original TPA results using the composition which included methane. FIGURE 4.1 shows the pressure traces from the TPA and compared to the measured data for Blend 1 and Blend 3 when using the default values of multipliers (uncalibrated) for the heat transfer and valve area (which were equal to 1).

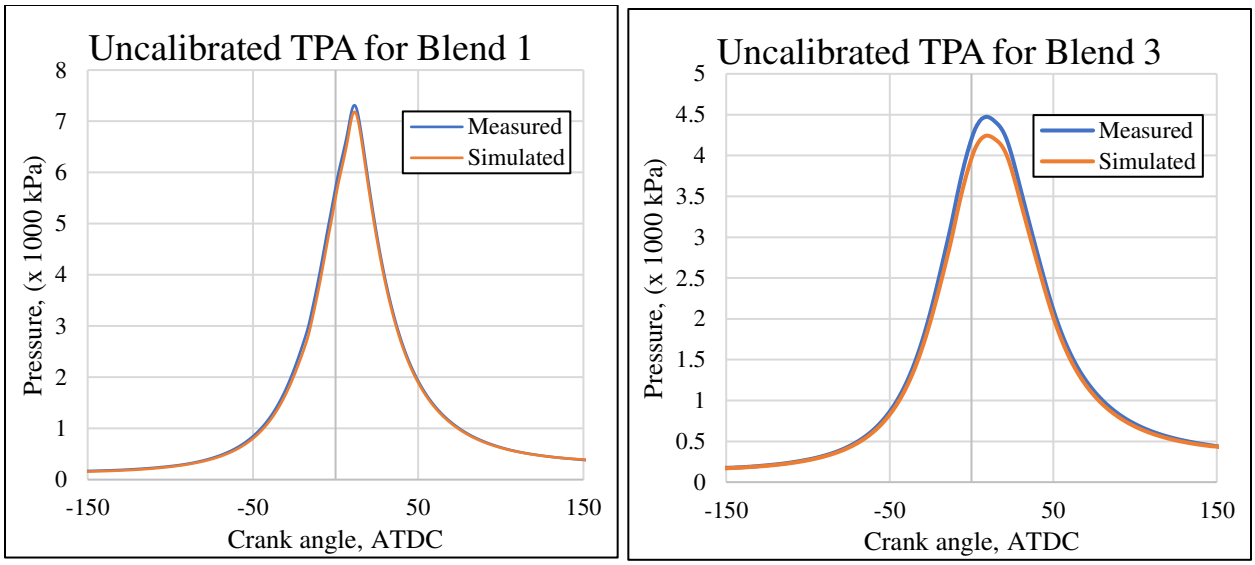


**FIGURE 4.1**: Pressure traces for uncalibrated TPA for Blend 1 (40°C blend) at CR = 12.14, spark timing = -19 ATDC (left) and Blend 3 (90°C blend) at CR = 10.65, spark timing = -17 ATDC (right)

The uncalibrated TPA results might not always match the experimental results, depending on if the default multipliers in the model were sufficient to simulate the physical and thermodynamical phenomenon inside the engine. The pressure trace from the uncalibrated TPA for Blend 1 appears to match closely with the measured data. But there is a noticeable difference between the pressure traces obtained from the TPA and the measured pressure data for Blend 3. This higher deviation for Blend 3 could be caused by the default multipliers being insufficient to model the highly dilute mixture combustion. Other factors can include slight inconsistencies during collection of experimental data and modelling complications due to the very low heating value of the fuel mixture. However, a significant deviation of the simulated pressure trace from the measured pressure trace would give inaccurate results for the prediction of trapped mass. To make the TPA output results better for both blends, the heat transfer multipliers for the intake and exhaust ports and the in-cylinder convection multiplier were adjusted. The flow area multipliers of the intake and exhaust valves were also changed to match the measured data for trapped mass in the cylinder. FIGURE 4.2 shows the pressure traces of the TPA and measured data after the changes were made to the multipliers. The values of the multipliers for the two blends are shown in TABLE A3.1 and TABLE A3.2 in Appendix 3. The values of trapped mass per cycle also matched better with an average error of less than 5% for all the

available cases for Blend 1. The errors for the same parameters for Blend 3 were slightly higher than blend 1 but since they were close to the aimed 5% error, these simulated data points were considered acceptable.

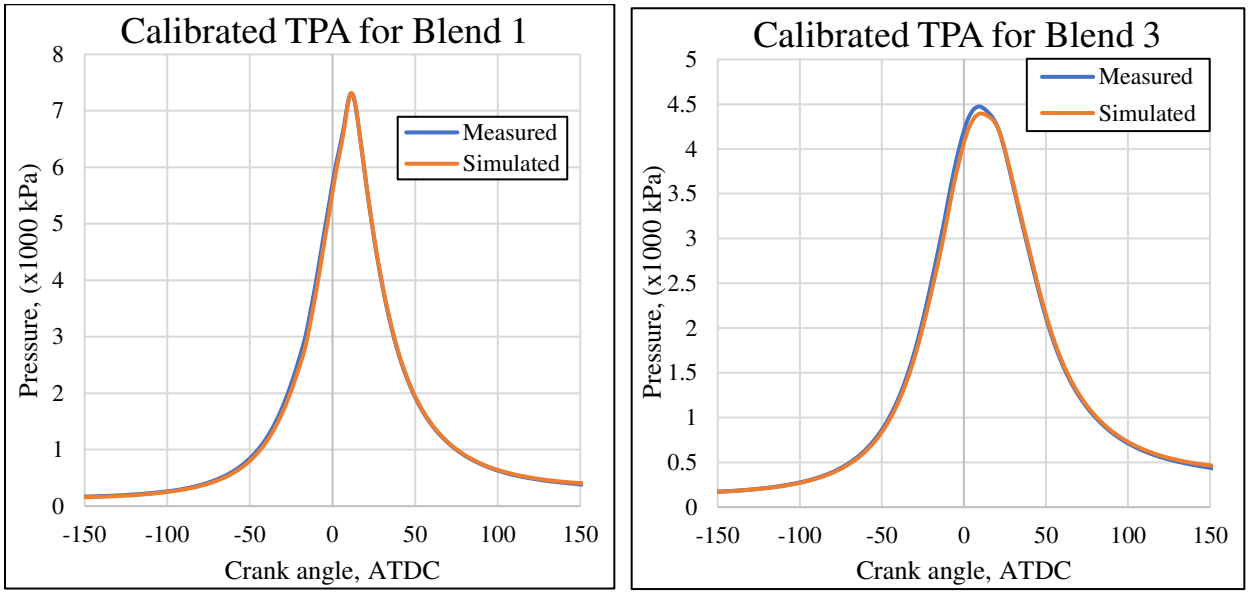


**FIGURE 4.2:** Pressure traces from calibrated TPA for Blend 1 (40°C blend) at CR = 12.14, spark timing = -19 ATDC (left) and Blend 3 (90°C blend) at CR = 10.65, spark timing = -17 ATDC (right)

## 4.2 Measured + Predicted (M+P) Model Results

After the completion of the TPA, the combustion model is included in the GT-POWER model. The coefficient values of eqn. 3.5 used to model the laminar flame speeds for each of the mechanisms employed in the combustion model of the different blends (procedure explained in section 3.2.3.1) are shown in TABLE 3.5 and TABLE 3.6. The M+P model allows the optimization runs on the model by the IDO to get the turbulent flame multipliers (i.e., $C_{FKG}$, $C_{TFS}$, and $C_{TLS}$) used in Eqn. 3.10 – 3.13. The IDO outputs the values of the turbulent flame multipliers by using the data from the calibration points (as explained in section 3.3). TABLE 4.1 and TABLE 4.2 show the values of the multipliers obtained from the optimization runs for Blend 1 and Blend 3 for each of the mechanisms used in the study. FIGURE 4.3 and FIGURE 4.4 show the predicted values of the pressure traces for a data point after the calibration in the M+P model for the chemical mechanisms used.

The differences in the optimized multiplier values based on the chemical mechanisms can be seen in these tables. As different chemical mechanisms model the combustion differently, the flame speeds obtained from each of the mechanisms was slightly different from each other. This affects the burn rates in the engine and thus, each chemical mechanism had a different set of turbulent flame multipliers to model the syngas mixture combustion. However, similarities could be seen in the multiplier values. For example, the Flame Kernel Growth Multiplier ($C_{FKG}$) had a fairly uniform value of 2.99 over all the mechanisms and blends used. For Blend 1 the value of $C_{TLS}$ was also fairly constant near the value of 0.5. Blend 3 showed a nearly constant value for $C_{TFS}$ (around 2.99) for all the three mechanisms. To ascertain which mechanism multipliers give the best predictions, the results must be compared to the withheld data. This is done during the validation of the model.

**TABLE 4.1**: Optimized turbulent flame multipliers for Blend 1 (40°C blend) when using San Diego mechanism, GRI mechanism, and NUIG syngas mechanism

| | **San Diego** | **GRI** | **NUIG-Syngas** |
|---|---|---|---|
| Flame Kernel Growth Multiplier ($C_{FKG}$) | 2.993461 | 2.999996 | 2.990364 |
| Turbulent Flame Speed Multiplier ($C_{TFS}$) | 0.614423 | 0.885543 | 0.824079 |
| Taylor Length Scale Multiplier ($C_{TLS}$) | 0.500241 | 0.500118 | 0.500049 |

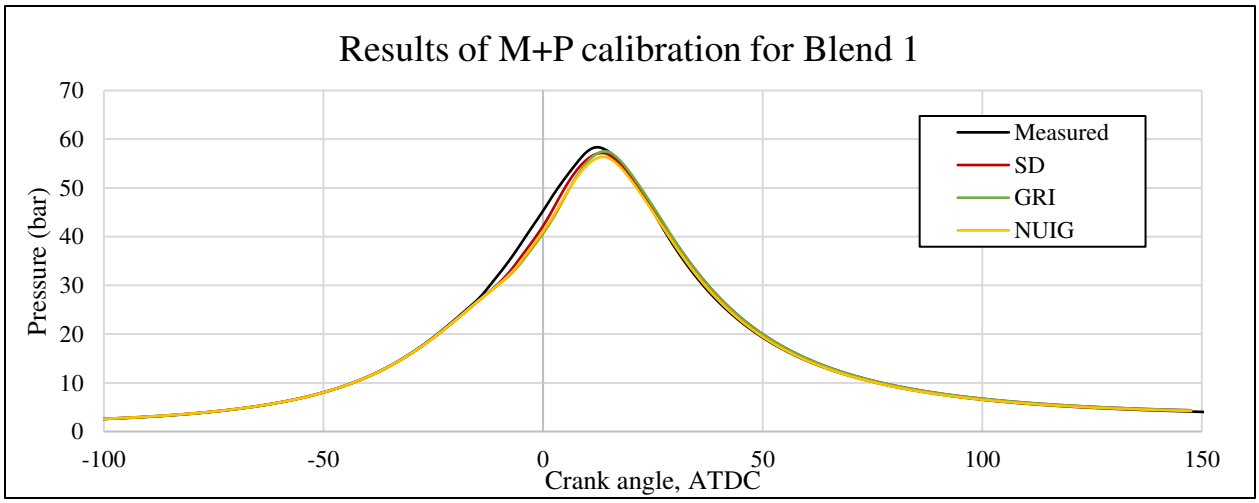


**FIGURE 4.3:** Comparison of the measured pressure trace with results of the M+P optimization when using different mechanisms for Blend 1 (40°C blend) for CR = 10.65 and spark timing = -17 ATDC

**TABLE 4.2:** Optimized turbulent flame multipliers for Blend 3 (90°C blend) when using San Diego mechanism, GRI mechanism, and NUIG syngas mechanism

| | San Diego | GRI | NUIG-Syngas |
|---|---|---|---|
| Flame Kernel Growth Multiplier ($C_{FKG}$) | 2.9997096 | 2.9998963 | 2.9999425 |
| Turbulent Flame Speed Multiplier ($C_{TFS}$) | 2.9996946 | 2.9995182 | 2.999795 |
| Taylor Length Scale Multiplier ($C_{TLS}$) | 2.8003767 | 1.6747065 | 2.1203704 |

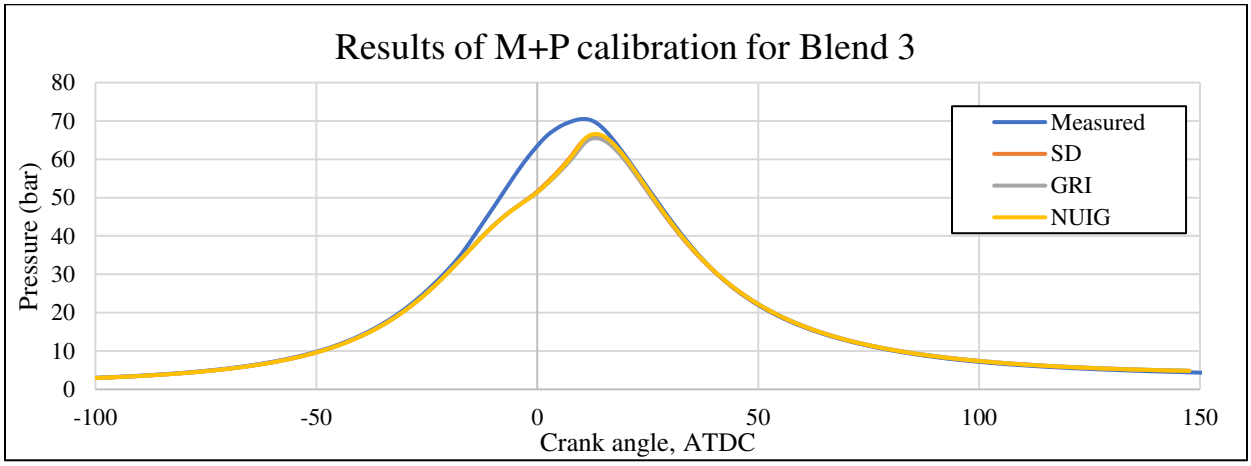


**FIGURE 4.4:** Comparison of the measured pressure trace with results of the M+P optimization when using different mechanisms for Blend 3 (90°C blend) for CR = 12.86 and spark timing = -21 ATDC

## 4.3 Validation of the predictive model

By including the attributes used to model the turbulent combustion of the engine in the combustion model, the predictive combustion model for the CFR engine is completed. To validate the predictive nature of the model, simulations were performed using the conditions of the withheld operating points and compared to the experimental results. In this study, the final model results were compared with the withheld data points (3 for each blend) representing different compression ratios, spark timings, and operating speeds of the engine. The data points withheld for Blend 1 and Blend 3 are shown in the TABLE 4.3 – 4.8. The tables also show the comparison of the predicted data with the measured parameters for the different blends when using different chemical mechanisms. FIGURE 4.5 and FIGURE 4.6 show the predicted pressure traces for the withheld data points when using different chemical mechanisms for the different blends.

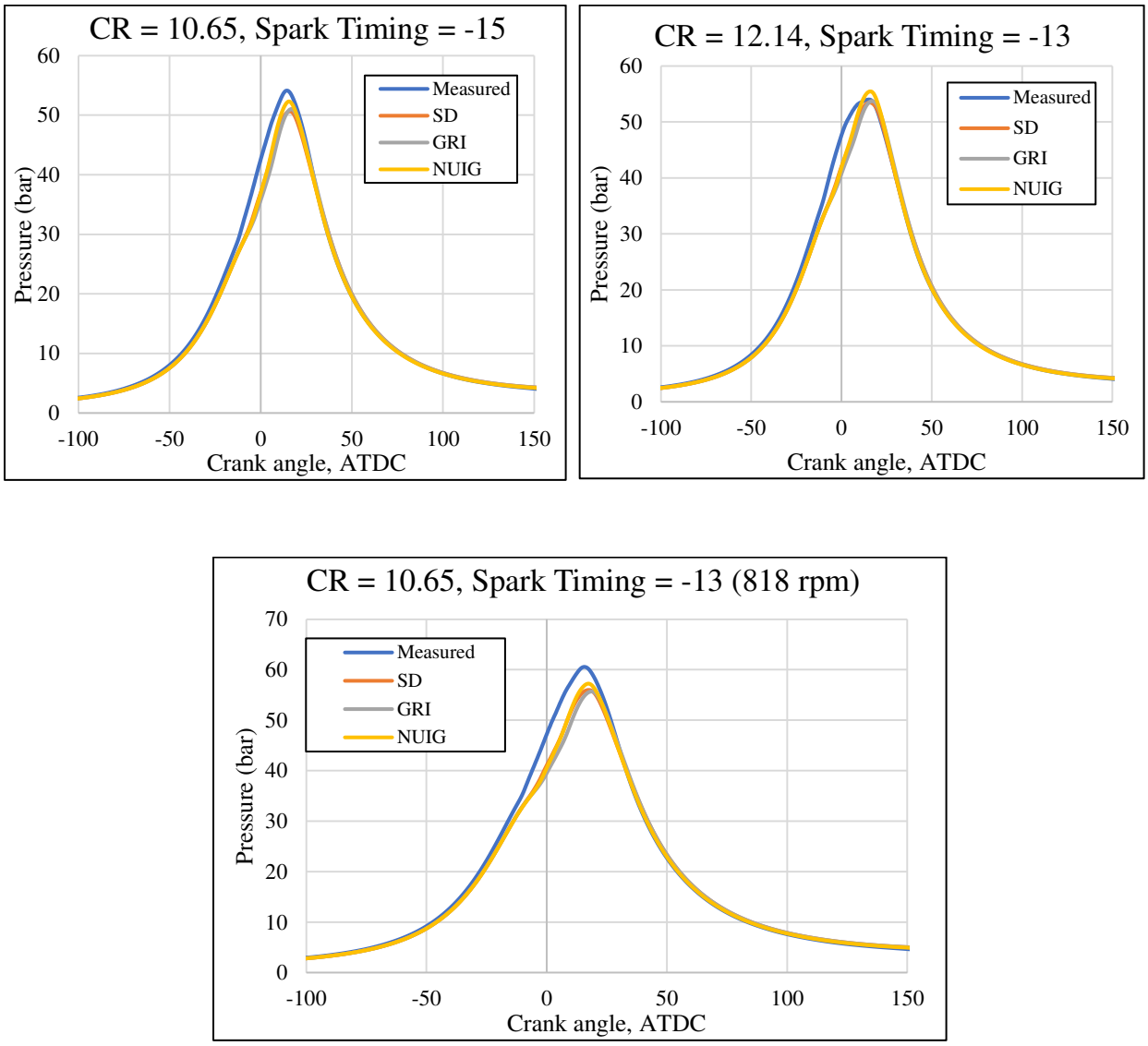


**FIGURE 4.5**: Pressure traces from predictive model using different chemical mechanisms for the validation data points for Blend 1 (40°C blend)

**TABLE 4.3:** Error percentage comparisons for Blend 1 (40°C blend) using the San Diego mechanism

| Operating condition | CR = 10.65, -15 ST | CR = 12.14, -13 ST | CR = 10.65, -13 ST (818 rpm) | Average error % |
|---|---|---|---|---|
| **Brake Power [kW]** | -2.46% | 3.55% | 3.87% | 3.29% |
| **Indicated Power [kW]** | 1.86% | 5.11% | 3.60% | 3.53% |
| **IMEP (gross) (kPa)** | 4.64% | 7.07% | 4.67% | 5.46% |
| **Air intake (mg/cyl)** | -5.08% | -4.00% | -5.25% | 4.78% |
| **Fuel intake (mg/cyl)** | 0.90% | 0.19% | 3.08% | 1.39% |

**TABLE 4.4:** Error percentage comparisons for Blend 1(40°C blend) using the GRI mechanism

| Operating condition | CR = 10.65, -15 ST | CR = 12.14, -13 ST | CR = 10.65, -13 ST (818 rpm) | Average error % |
|---|---|---|---|---|
| **Brake Power [kW]** | -2.46% | 3.55% | 3.87% | 3.29% |
| **Indicated Power [kW]** | 1.86% | 5.11% | 3.60% | 3.53% |
| **IMEP (gross) (kPa)** | 4.96% | 7.45% | 4.84% | 5.75% |
| **Air intake (mg/cyl)** | -5.07% | -4.00% | -5.22% | 4.76% |
| **Fuel intake (mg/cyl)** | 0.91% | 0.19% | 3.11% | 1.41% |

**TABLE 4.5:** Error percentage comparisons for Blend 1(40°C blend) using the NUIG-syngas mechanism

| Operating condition | CR = 10.65, -15 ST | CR = 12.14, -13 ST | CR = 10.65, -13 ST (818 rpm) | Average error % |
|---|---|---|---|---|
| **Brake Power [kW]** | -2.46% | -1.16% | -0.29% | 1.30% |
| **Indicated Power [kW]** | -0.75% | 2.48% | 3.60% | 2.28% |
| **IMEP (gross) (kPa)** | 3.17% | 5.74% | 3.20% | 4.03% |
| **Air intake (mg/cyl)** | -7.84% | -6.81% | -7.99% | 7.55% |
| **Fuel intake (mg/cyl)** | 4.41% | 3.66% | 6.69% | 4.92% |

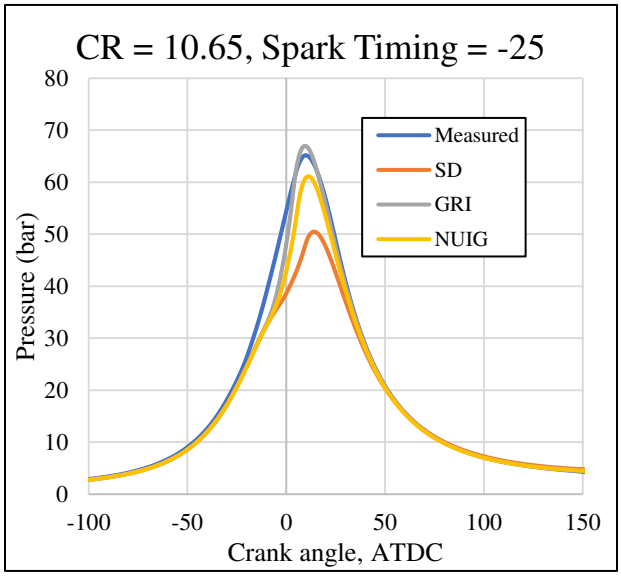


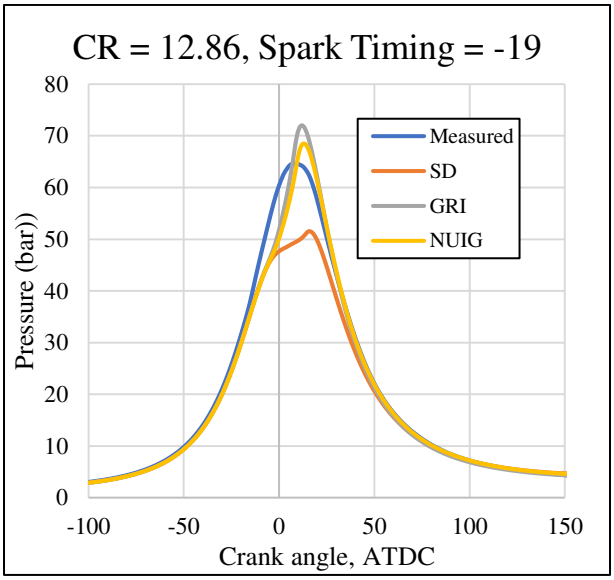

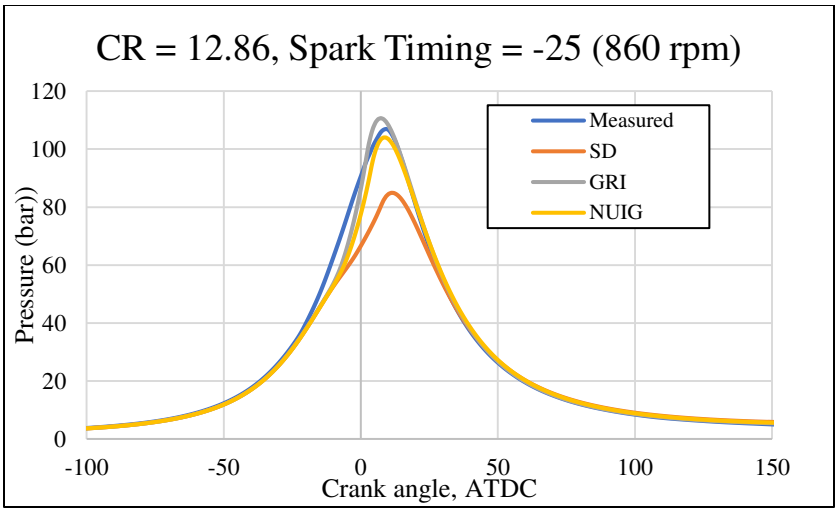


**FIGURE 4.6**: Pressure traces from predictive model using different chemical mechanisms for the validation data points for Blend 3 (90°C blend)

**TABLE 4.6:** Error percentage comparisons for Blend 3 (90°C blend) using the San Diego mechanism

| Operating condition | CR = 10.65, -25 ST | CR = 12.86, -19 ST | CR = 12.86, -25 ST (860 rpm) | Average error % |
|---|---|---|---|---|
| **Brake Power [kW]** | -21.58% | -29.93% | 26.70% | 26.07% |
| **Indicated Power [kW]** | -9.84% | -15.78% | -13.05% | 12.89% |
| **IMEP (gross) (kPa)** | 16.94% | -10.11% | 3.80% | 10.28% |
| **Air intake (mg/cyl)** | 0.04% | -0.50% | 18.44% | 6.33% |
| **Fuel intake (mg/cyl)** | 0.04% | -0.50% | 17.67% | 6.07% |

**TABLE 4.7:** Error percentage comparisons for Blend 3 (90°C blend) using the GRI mechanism

| Operating condition | CR = 10.65, -25 ST | CR = 12.86, -19 ST | CR = 12.86, -25 ST (860 rpm) | Average error % |
|---|---|---|---|---|
| **Brake Power [kW]** | -1.98% | -9.91% | 36.08% | 15.99% |
| **Indicated Power [kW]** | 0.18% | -0.47% | -9.27% | 3.30% |
| **IMEP (gross) (kPa)** | 4.20% | 3.04% | 8.47% | 5.23% |
| **Air intake (mg/cyl)** | -0.60% | -1.55% | 17.04% | 6.40% |
| **Fuel intake (mg/cyl)** | -0.60% | -1.55% | 16.27% | 6.14% |

**TABLE 4.8:** Error percentage comparisons for Blend 3 (90°C blend) using the NUIG-syngas mechanism

| Operating condition | CR = 10.65, -25 ST | CR = 12.86, -19 ST | CR = 12.86, -25 ST (860 rpm) | Average error % |
|---|---|---|---|---|
| **Brake Power [kW]** | -11.78% | 0.10% | 40.78% | 17.55% |
| **Indicated Power [kW]** | -4.83% | 2.08% | -7.38% | 4.76% |
| **IMEP (gross) (kPa)** | 0.35% | 7.01% | 10.81% | 6.06% |
| **Air intake (mg/cyl)** | -6.54% | -9.31% | 11.17% | 9.01% |
| **Fuel intake (mg/cyl)** | 4.78% | 7.74% | 23.79% | 12.11% |

It can be seen that the model has better prediction of the engine performance when using Blend 1 when compared to Blend 3. FIGURE 4.5 shows that the model slightly under-predicts the peak pressures associated with each of the withheld data points for Blend 1. The under prediction of the peak pressures is consistent for the different blends irrespective of the mechanism used. The deviation of the predicted pressure traces is more pronounced for Blend 3 and can be seen in FIGURE 4.6. The peak pressures of San Diego mechanism appears to be significantly lower than the peak pressures of the CFR engine. The other mechanisms (i.e., GRI and NUIG-syngas) appear to give varying predictions for the peak pressures for the different operating conditions. A source of this deviation in results could be the difference in the trapped mass between the model and the experiments. TABLE 4.3 to 4.8 show that the air intake in the model is lower than the experiments. This could be causing incomplete combustion of the fuel and thus a lesser heat release. The lower air intake could also be resulting in lower in-cylinder pressures and thus additional deviation in the results. Minor flaws in the heat transfer model inside the engine could also be a major contributor of such uncertainties and errors in the model. For Blend 3, the controlling the flow of the steam into the intake stream is quite complicated and can be a major source of uncertainty in measuring the intake composition of the engine. As water has a significant percentage for Blend 3, the higher uncertainty in the water flow could also be a potential cause for the model predictions to have higher deviations from the corresponding measured data.

The model was also intended to predict operating points that would cause knocking in the engine with the syngas fuel blend. It can be seen in FIGURE 4.7 and 4.8 that the model was able to predict the knock in the CFR engine for both the blends at the measured operating points when the NUIG mechanism was used. The NUIG syngas mechanism, however, was not completely perfect for the knock prediction application. The mechanism predicted knock for Blend 1 at a CR of 12.14 and spark timing of 19° BTDC when no knock was observed in the experimental data. For Blend 3, the NUIG syngas mechanism did not predict knock at a CR of 12.86 and spark timing of 27° BTDC. Knock was detected at this operating condition during experimentation. The mechanism did however show a trend in the knock index magnitude similar to the experimental data. As the procedure for determining the values of the KI are different in the experimental methods and in GT-POWER, it is not surprising that the KI values are not the same. Since the increase in the KI values were similar, the results were considered acceptable to be able to predict knock in the engine using the syngas blends.

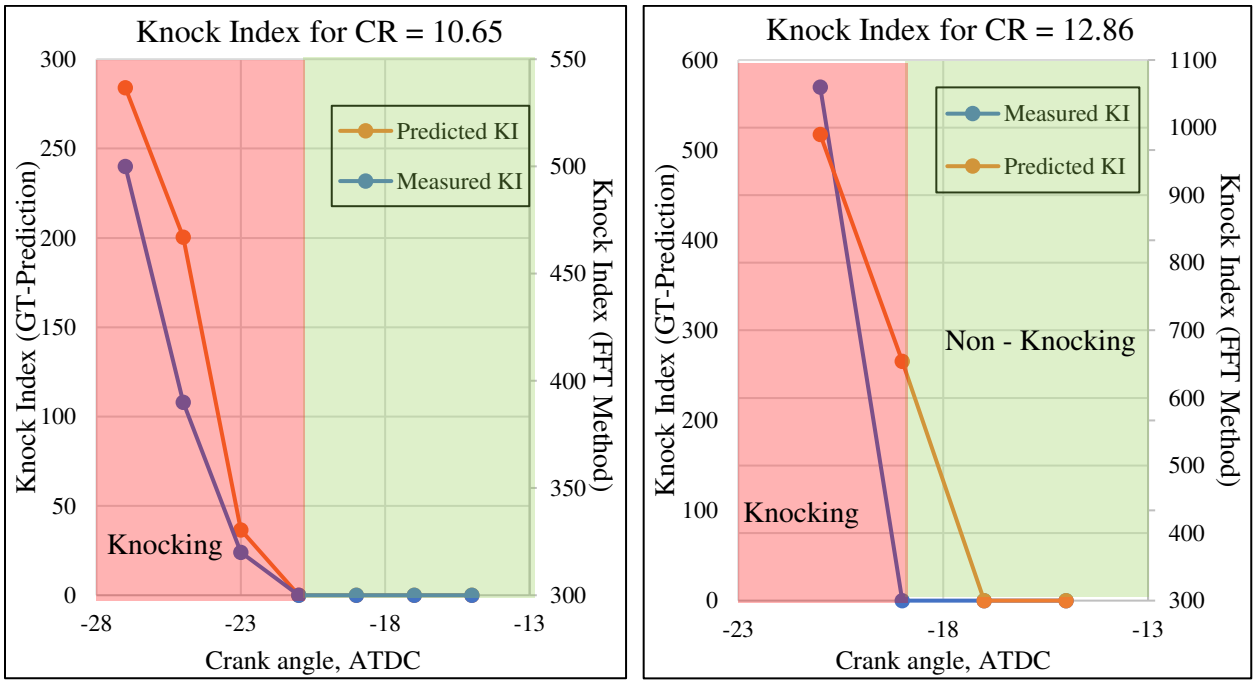


**FIGURE 4.7**: Knock Index (KI) predictions by the model for Blend 1(40°C blend) at CR = 10.65 (left) and CR = 12.86 (right) when using the NUIG-syngas mechanism

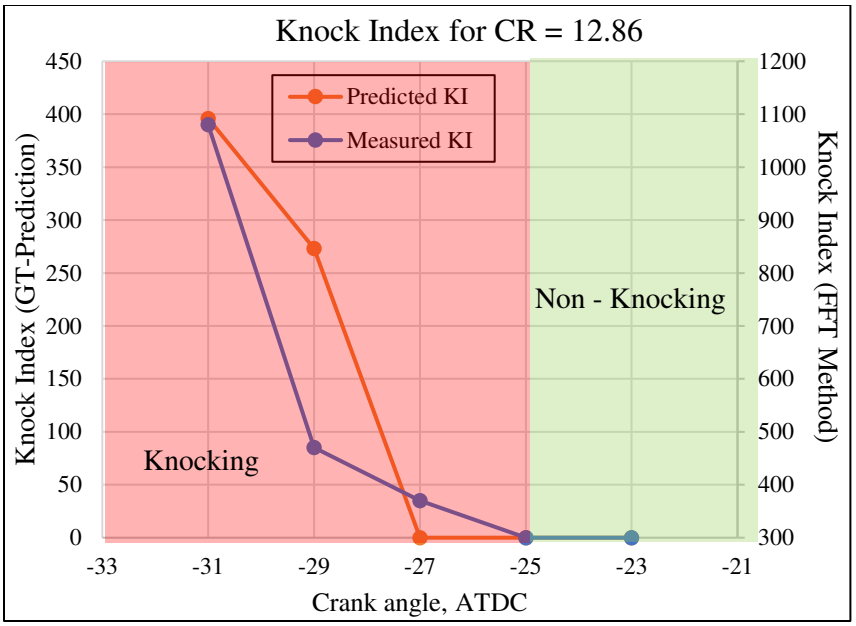


**FIGURE 4.8**: Knock Index (KI) predictions by the model for Blend 3 (90°C blend) when using the NUIG-syngas mechanism

The other two mechanisms (i.e., San Diego mechanism and the GRI mechanism) were not very successful in predicting knock in the CFR engine. Upon using these two mechanisms, knock is predicted in the model at greater advanced spark timings than those measured in the experiment. To initiate knock in the model at the same operating points as in the experiments, more aggressive conditions (e.g., increased wall temperatures and higher intake gas temperatures) had to be imposed when using the San Diego and GRI mechanisms. This method of inducing knock in the model just to match the experimental results does no good when trying to develop a predictive model. Since the initial conditions from the TPA are essentially the same for each mechanism used, it can be clearly seen that chemical kinetics plays an important role in the knock prediction in the model. Another explanation for the inability of the San Diego and GRI mechanisms to predict knock could be the way those mechanisms were developed. As mentioned earlier, these two mechanisms were primarily developed for combustion of natural gas and methane. Since the fuel used in this study has minimal amounts of methane (<1%), it could be possible that these mechanisms do not completely capture the combustion occurring in the syngas. It was anticipated that since these mechanisms are often used to model combustion phenomenon, these should also be able to model the syngas combustion. This turned out to be partially true during the validation runs using data of the withheld

operating points, as the percentage errors when using these mechanisms were also quite low indicating good predictability from the model. However, this was not the case during the knock analysis. A possible cause for this observation could be the way the fuel is defined in both instances. As explained in section 3.2.1.1, different definitions were used to describe the fuel in GT-POWER when comparing the engine performance predictions and knock predictions. During the engine performance runs, the FluidMixtureCombined definition combined the constituents into a single fuel to match the properties interpolated from the entire mixture. When using the mechanisms in this fuel definition, the syngas blends could be modelled as a generic fuel, like natural gas, with a fixed heating value and thus lead to the closely predictive results. However, during the knock prediction the FluidMixture definition distinguishes the individual constituents of the mixture and could cause chemical kinetics of individual species to play a greater role during the knock prediction. Since these mechanisms are intended for combustion of a different mixture, knocking in the syngas mixture may not have been predicted. The NUIG-Syngas mechanism on the other hand was specifically built to model hydrogen-syngas combustion. Hydrogen is the major combustive entity in the syngas mixture considered in this study. Even though the mechanism lacks any reactions for methane combustion, the absence of a minor species might not be drastically affecting the simulation results when compared to the measured data and the results when using other mechanisms. This can be seen from the low errors in TABLE 4.9 and 4.12. The hydrogen syngas mechanism resulted in predicting knock better than the other two mechanisms, possibly due to the same reasons mentioned earlier. Due to these factors, it was decided to use the hydrogen syngas mechanism from NUIG as the preferred chemical mechanism to model the syngas mixture combustion in GT-POWER in this study.

# Chapter 5: Conclusions and Future Work

## 5.1 Conclusions

The main objective of this study was to use GT-POWER and CHEMKIN and develop a virtual model of the CFR engine present at the Powerhouse facility of Colorado State University to predict the combustion of a dilute syngas fuel, in this case from a SOFC. The tail gas composition from the SOFC was to be modified such that it could become a viable syngas fuel to be used in the CFR engine. The model was intended to be able to predict the combustion and performance of the CFR engine when operating on the syngas blends with varying amounts of water dilution and to also predict knock in the engine at different operating conditions. The outcome of this study can be summarized in the following points:

1. The stock tail-gas composition from the SOFC was modified to increase the energy density of the syngas to be used as fuel in the CFR engine. The stock tail-gas was cooled to allow for condensation of water in the mixture and the final composition of water in the mixture was calculated for different degrees of cooling. Concept of partial pressures and relative humidity was used to determine the final compositions of the syngas blends used. Subsequent simulations were done using these syngas blends calculated. The syngas blends appear to have higher flame speeds than methane at elevated temperatures (> 650 K) for most of the syngas blends and mechanisms used (i.e., San Diego and GRI mechanism). This indicates the syngas blends can be more reactive than methane at these elevated temperatures. However, this doesn't translate to higher efficiency for syngas blends (when compared to methane) when used in the engine as the energy density of methane is significantly higher. No comparison was made for the syngas blends and methane using the NUIG-syngas mechanism as there are no reactions of methane included in the mechanism.
2. A simplified virtual model of the CFR engine was successfully developed in GT-POWER. The focus of the model design was the cylinder combustion chamber and the components directly connected to it. Effects of other components (e.g., turbocharger, runner manifolds etc.) were

implicitly defined in the virtual model. This allowed for reduced computational effort during simulations and ensured the model was easily constructed to emulate the experiments. The developed model also included a combustion model (with inputs from CHEMKIN) of the CFR engine which was capable of simulating the combustion of the syngas blends in the CFR engine.

3. The developed model was calibrated using tools present in GT-POWER (e.g. TPA runs, M+P analysis, IDO runs) and resulted in a predictive model of the engine. The model was developed to predict the performance and knocking of the engine at different operating conditions while using different syngas blends without making changes to the input parameters.
4. Performance predictions (TABLE 4.3 – 4.8) and knock predictions (FIGURE 4.7 – 4.8) from the model were compared with the experimental data. The model was able to predict performance characteristics of the engine quite closely to the experimental data (within estimated experimental uncertainties of ~5%) when using Blend 1 as the fuel. Predictions of performance characteristics for Blend 3 exhibited higher deviations (> 5%) from the measurements. Potential causes include difficulty in modelling a very dilute fuel mixture and possibly some inconsistencies in measured data. However, the trend for knock predictions follow similar trends for both the blends.
5. The focus on hydrogen combustion in the NUIG-syngas mechanism appeared to replicate the syngas combustion better than the other two mechanisms and thus give better knock results. The San Diego and the GRI mechanism were designed for methane/natural gas combustion and so could be lacking fidelity in reactions essential for knock prediction with $H_2$ and CO fuels.

## 5.2 Future Work

The predictive model developed in this study, although able to emulate the CFR engine tests, is not perfect. Further work can be done to reduce the errors in the model output. One way would be to improve the heat transfer model used for the model. As the heat transfer model is the biggest source of uncertainty in the simulation, reduction in the uncertainty would help improve the results. This can be done by performing additional adjustments to the multipliers governing the heat transfer in the engine. Another way to improve

the predictive model would be to choose better chemical mechanisms to model the syngas combustion. AS shown in this study, the choice of chemical mechanism can have significant effects on the results of the simulation. Additional reactions can be added to the current NUIG-syngas mechanism to incorporate methane combustion. This would ensure the mechanism can be used even if there is a change in the syngas composition that would lead to an increase in methane content. Apart from improving the NUIG-syngas mechanism, other syngas mechanisms (e.g. Davis 2005 [48], Li et al., [25]) can also be explored to determine the suitability of usage for similar conditions. Changes in mechanism can cause changes in the flame speeds of the mixture. In the current study, the flame speeds obtained from CHEMKIN varied for different mechanisms for the same conditions. Experimentally determining the laminar flame speeds of the syngas mixtures at different pressures and temperatures would allow for quantitative comparison with the flame speeds output from CHEMKIN which could help determine the mechanism which would model the syngas combustion better. Also, the equation used by GT-POWER could not exactly match the laminar flame speed values obtained from CHEMKIN. An alternate route which can be explored is to use a look-up table that clearly mentions the flame speed of the mixture at different conditions of pressure and temperature. This would reduce the uncertainty in laminar flame speeds currently described by the coefficients in the eqn. 3.5. This would however depend on the ability of GT-POWER to incorporate the table into its calculations during the simulation runs.

# References

[1] Cho, H. M., and He, B.-Q., 2007, "Spark ignition natural gas engines—A review," Energy conversion and management, 48(2), pp. 608-618.

[2] Murugesan, A., Umarani, C., Subramanian, R., and Nedunchezhian, N., 2009, "Bio-diesel as an alternative fuel for diesel engines—a review," Renewable and sustainable energy reviews, 13(3), pp. 653-662.

[3] Sridhar, G., Paul, P., and Mukunda, H., 2001, "Biomass derived producer gas as a reciprocating engine fuel—an experimental analysis," Biomass and Bioenergy, 21(1), pp. 61-72.

[4] Hagos, F. Y., Aziz, A. R. A., and Sulaiman, S. A., 2014, "Trends of syngas as a fuel in internal combustion engines," Advances in Mechanical Engineering, 6, p. 401587.

[5] Chacartegui, R., Torres, M., Sánchez, D., Jiménez, F., Muñoz, A., and Sánchez, T., 2011, "Analysis of main gaseous emissions of heavy duty gas turbines burning several syngas fuels," Fuel Processing Technology, 92(2), pp. 213-220.

[6] Shah, A., Srinivasan, R., D. Filip To, S., and Columbus, E. P., 2010, "Performance and emissions of a spark-ignited engine driven generator on biomass based syngas," Bioresource Technology, 101(12), pp. 4656-4661.

[7] Hulbert, M. C., 2017, "Modeling the Impact of Natural Gas Variation on Combustion in a Dual Fuel Engine," Illinois Institute of Technology.

[8] Azimov, U., Tomita, E., Kawahara, N., and Harada, Y., 2011, "Effect of syngas composition on combustion and exhaust emission characteristics in a pilot-ignited dual-fuel engine operated in PREMIER combustion mode," International Journal of Hydrogen Energy, 36(18), pp. 11985-11996.

[9] Spaeth, C. T., 2012, "Performance characteristics of a diesel fuel piloted syngas compression ignition engine."

[10] Withrow, L., and Rassweiler, G. M., 1936, "Slow motion shows knocking and non-knocking explosions," SAE Transactions, pp. 297-303.

[11] Poulos, S. G., and Heywood, J. B., 1983, "The effect of chamber geometry on spark-ignition engine combustion," SAE transactions, pp. 1106-1129.

[12] Kamimoto, T., and Kobayashi, H., 1991, "Combustion processes in diesel engines," Progress in Energy and Combustion Science, 17(2), pp. 163-189.

[13] GT-Suite, "Engine Performance Application Manual, Version 2018."

[14] "Gamma Technologies Home Page, https://www.gtisoft.com."

[15] P McCrady, J., C Hansen, A., and Lee, C.-F., 2007, "Modeling Biodiesel Combustion Using GT-Power," 2007 ASAE Annual Meeting.

[16] Etheridge, J., Mosbach, S., Kraft, M., Wu, H., and Collings, N., 2011, "Modelling cycle to cycle variations in an SI engine with detailed chemical kinetics," 158(1), pp. 179-188.

[17] Noda, T., Hasegawa, K., Kubo, M., and Itoh, T., 2004, "Development of Transient Knock Prediction Technique by Using a Zero-Dimensional Knocking Simulation with Chemical Kinetics," SAE International.

[18] Pal, P., Kolodziej, C. P., Choi, S., Som, S., Broatch, A., Gomez-Soriano, J., Wu, Y., Lu, T., and See, Y. C., 2018, "Development of a Virtual CFR Engine Model for Knocking Combustion Analysis," SAE International Journal of Engines, SAE International, pp. 1069-1082.

[19] Choi, S., Kolodziej, C. P., Hoth, A., and Wallner, T., 2018, "Development and Validation of a Three Pressure Analysis (TPA) GT-Power Model of the CFR F1/F2 Engine for Estimating Cylinder Conditions," SAE International.

[20] Tsuchiyama, T., Kuboyama, T., Moriyoshi, Y., Kiura, T., Koga, H., and Aoki, T., 2016, "1-D Simulation Model Developed for a General Purpose Engine," SAE International.

[21] Kulkarni, A. M., Shaver, G. M., Popuri, S. S., Frazier, T. R., and Stanton, D. W., 2010, "Computationally efficient whole-engine model of a Cummins 2007 turbocharged diesel engine," Journal of Engineering for Gas Turbines and Power, 132(2), p. 022803.

[22] Natarajan, J., Kochar, Y., Lieuwen, T., and Seitzman, J., 2009, "Pressure and preheat dependence of laminar flame speeds of H2/CO/CO2/O2/He mixtures," 32(1), pp. 1261-1268.

[23] He, Y., Wang, Z., Yang, L., Whiddon, R., Li, Z., Zhou, J., and Cen, K., 2012, "Investigation of laminar flame speeds of typical syngas using laser based Bunsen method and kinetic simulation," 95, pp. 206-213.

[24] Das, A. K., Kumar, K., and Sung, C.-J., 2011, "Laminar flame speeds of moist syngas mixtures," 158(2), pp. 345-353.

[25] Li, J., Zhao, Z., Kazakov, A., Chaos, M., Dryer, F. L., and Scire Jr, J. J., 2007, "A comprehensive kinetic mechanism for CO, CH2O, and CH3OH combustion," International Journal of Chemical Kinetics, 39(3), pp. 109-136.

[26] Ghojel, J. I., 2010, "Review of the development and applications of the Wiebe function: A tribute to the contribution of Ivan Wiebe to engine research," International Journal of Engine Research, 11(4), pp. 297-312.

[27] Cordeiro de Melo, T. C., Machado, G. B., Machado, R. T., Pereira Belchior, C. R., and Pereira, P. P., 2007, "Thermodynamic Modeling of Compression, Combustion and Expansion Processes of Gasoline, Ethanol and Natural Gas with Experimental Validation on a Flexible Fuel Engine."

[28] Cooney, C., Worm, J., Michalek, D., and Naber, J., 2008, "Wiebe function parameter determination for mass fraction burn calculation in an ethanol-gasoline fuelled SI engine," Journal of KONES, 15, pp. 567-574.

[29] Borg, J. M., and Alkidas, A. C., 2008, "Investigation of the Effects of Autoignition on the Heat Release Histories of a Knocking SI Engine Using Wiebe Functions."

[30] Lindström, F., Ångström, H.-E., Kalghatgi, G., and Möller, C. E., 2005, "An Empirical SI Combustion Model Using Laminar Burning Velocity Correlations," SAE Transactions, 114, pp. 833-846.

[31] Waukesha, "CFR F-1 & F-2. Research Method (F-1),Motor Method (F-2), Octane Rating Units. Operation & Maintenance Manual."

[32] Wise, D. M., 2013, "INVESTIGATION INTO PRODUCER GAS UTILIZATION IN HIGH PERFORMANCE NATURAL GAS ENGINES," Doctor of Philosophy, Colorado State University.

[33] Millo, F., and Ferraro, C., 1998, "Knock in SI engines: a comparison between different techniques for detection and control," SAE transactions, pp. 1091-1112.

[34] Diaz, G. J. A., Martinez, L. M. C., Montoya, J. P. G., and Olsen, D. B., 2019, "Methane number measurements of hydrogen/carbon monoxide mixtures diluted with carbon dioxide for syngas spark ignited internal combustion engine applications," Fuel, 236, pp. 535-543.

[35] Braun, R. J., Sullivan, N., Vincent, T., Danforth, R., Bandhauer, T., Olsen, D., Windom, B., and Schaffer, B., "Development Of A Novel High Efficiency, Low Cost Hybrid SOFC/Internal Combustion Engine Power Generator," Proc. 16th International Symposium on SOFCs.

[36] Ferguson, C. R., and Kirkpatrick, A. T., 2016, Internal Combustion Engines - Applied Thermosciences, John Wiley & Sons, Ltd.

[37] Aslam, M., Masjuki, H., Kalam, M., Abdesselam, H., Mahlia, T., and Amalina, M., 2006, "An experimental investigation of CNG as an alternative fuel for a retrofitted gasoline vehicle," Fuel, 85(5-6), pp. 717-724.

[38] "National Institute of Standards and Technology Chemistry WebBook, SRD 69, https://webbook.nist.gov/cgi/cbook.cgi?ID=C7732185&Mask=4&Type=ANTOINE&Plot=on#ANTOINE."

[39] Morganti, K. J., 2013, "A study of the knock limits of liquefied petroleum gas (LPG) in spark-ignition engines."

[40] Technologies, G., 2018, "GT-Suite, Flow Theory Manual."

[41] Heywood, J. B., 1988, Internal Combustion Engine Fundamentals, McGraw-Hill.

[42] Metzger, M., 2006, "Length and time scales of the near-surface axial velocity in a high Reynolds number turbulent boundary layer," International journal of heat and fluid flow, 27(4), pp. 534-541.

[43] ""Chemical-Kinetic Mechanisms for Combustion Applications", San Diego Mechanism web page, Mechanical and Aerospace Engineering (Combustion Research), University of California at San Diego (http://combustion.ucsd.edu).".

[44] Smith, G. P., Golden, D. M., Frenklach, M., Moriarty, N. W., Eiteneer, B., Goldenberg, M., Bowman, C. T., Hanson, R. K., Song, S., Gardiner, W. C., Jr., Lissianski, V. V., and Qin, Z., "GRI - Mech 3.0, http://www.me.berkeley.edu/gri_mech/."

[45] Keromnes, A., Metcalfe, W. K., Heufer, K. A., Donohoe, N., Das, A. K., Sung, C.-J., Herzler, J., Naumann, C., Griebel, P., Mathieu, O., Krejci, M. C., Petersen, E. L., Pitz, W. J., and Curran, H. J., 2013, "An experimental and detailed chemical kinetic modeling study of hydrogen and syngas mixture oxidation at elevated pressures, http://dx.doi.org/10.1016/j.combustflame.2013.01.001,"Combustion and Flame 160 (2013) 995–1011.

[46] Zhou, C.-W., Li, Y., Burke, U., Banyon, C., Somers, K. P., Khan, S., Hargis, J. W., Sikes, T., Petersen, E. L., AlAbbad, M., Farooq, A., Pan, Y., Zhang, Y., Huang, Z., Lopez, J., Loparo, Z., Vasu, S. S., and Curran, H. J., 2018, ""An experimental and chemical kinetic modeling study of 1,3-butadiene combustion: Ignition delay time and laminar flame speed measurements" C*ombustion and Flame* 197 (2018) 423–438.."

[47] Olm, C., Zsély, I. G., Varga, T., Curran, H. J., and Turányi, T., 2015, "Comparison of the performance of several recent syngas combustion mechanisms," Combustion and flame, 162(5), pp. 1793-1812.

[48] Davis, S. G., Joshi, A. V., Wang, H., and Egolfopoulos, F., 2005, "An optimized kinetic model of H2/CO combustion," Proceedings of the Combustion Institute, 30(1), pp. 1283-1292.

[49] Technologies, G., 2018, "GT-Suite, Engine Performance Application Manual."

# Appendix 1

## A1.1 Intake/Exhaust heat transfer

The heat transfer from fluids inside of pipes to their walls is calculated using a heat transfer coefficient. The heat transfer coefficient is calculated at every time step from the fluid velocity, the thermo-physical properties and the wall roughness. The heat transfer coefficient for smooth pipes is calculated using the Colburn analogy.

$$h_{g,smooth} = \left(\frac{1}{2}\right) * C_f * \rho * U_{eff} * C_p * Pr^{\left(-\frac{2}{3}\right)} \quad \text{… Eqn.A1.1}$$

where,

$h_{g,smooth}$ = heat transfer coefficient for smooth pipes

$C_f$ = Fanning friction factor of smooth pipe

ρ = density of fluid

$U_{eff}$ = effective velocity outside boundary layer

$C_p$ = specific heat of fluid

$Pr$ = Prandtl number

$$h_{g,rough} = h_g * \left(\frac{C_{f,rough}}{C_{f,smooth}}\right)^n \quad \text{… Eqn.A1.2}$$

where,

$h_{g,rough}$ = heat transfer coefficient for rough pipes

n= 0.68 * $Pr^{0.215}$

Flow losses in pipes due to friction along the walls are calculated automatically via a Fanning friction factor $(C_f)$ as a function of Reynolds number and the wall surface roughness.

For a Newtonian flow in laminar flow

$C_f = 16/Re_D$ ($Re_D < 2000$) … Eqn. A1.3

$Re_D$ = Reynolds number based on pipe diameter

## A1.2 In-cylinder heat transfer

The 'EngCylHeatTr' reference object allows the user to define which heat transfer model is used to calculate the in-cylinder heat transfer coefficient. In this thesis, the WoschniGT model is used. Details of the model (as described in the GT-POWER manual [49])are mentioned below. Also, equations for the convective heat transfer coefficient can be found below.

WoschniGT indicates that the in-cylinder heat transfer will be calculated by a formula which closely emulates the classical Woschni correlation without swirl (as described in Section 12.4.3 of "Internal Combustion Engine Fundamentals" by John B. Heywood. The temperature exponent was implemented as -0.5 for computational efficiency. This is no longer necessary with modern computers, but the value has not been changed to keep results consistent.). The most important difference lies in the treatment of heat transfer coefficients during the period when the valves are open, where the heat transfer is increased by inflow velocities through the intake valves and also by backflow through the exhaust valves. This option is recommended when measured swirl data is not available.

The convective heat transfer coefficient for the **Woschni*** models is defined as follows:

$$h_{c\ (Woschni)} = \frac{K_1 * p^{0.8} * w^{0.8}}{B^{0.2} * T^{K_2}} \quad \text{…Eqn. A1.4}$$

where,

$h_c$ = convective heat transfer coefficient

B = cylinder bore (m)

$K_1$ = 3.01426

$K_2$ = 0.5

P = cylinder pressure (kPa)

T = cylinder temperature (K)

w = average cylinder gas velocity (m/s)

$$w = C_1 * S_p + C_2 * \frac{V_d * T_r}{P_r * V_r} * (p - p_m)$$ … Eqn. A1.5

where,

$C_1$ & $C_2$= constants

$S_p$ = Mean piston speed (m/s)

$T_r$ =Working fluid temperature prior to combustion (K)

P = Instantaneous fluid pressure (kPa)

$P_m$ = motoring fluid pressure at same angle as p (kPa)

$P_r$ = working fluid pressure prior to combustion (kPa)

$V_d$ = displaced volume ($m^3$)

$V_r$ = working fluid volume prior to combustion ($m^3$)

$$C_1 = 2.38 + \min\left(\frac{\dot{m}_{in}}{m_{cyl} * f}, 1\right)$$ … Eqn. A1.6

where,

$\dot{m}$ = instantaneous mass flow rate, summed over valves and orifices through which flow is currently entering cylinder (kg,s)

$m_{cyl}$ = instantaneous cylinder mass (kg)

f = engine frequency (rev/s)

$C_2$ = 0 (during cylinder gas exchange and compression)

= 3.24 e-3 (during combustion and expansion)

# Appendix 2

As explained in section 3.3, the NUIG-syngas mechanism had to be modified to remove the OH* species in the chemical reactions. The study compared the speeds obtained from CHEMKIN when using the chemical mechanism with and without the OH* species. The comparison was done for Blend 1 and Blend 3 and the results are illustrated in the FIGURE A2.1 and FIGURE A2.2 respectively. As it can be seen, there is no distinguishable difference in the flame speeds between the two mechanisms.

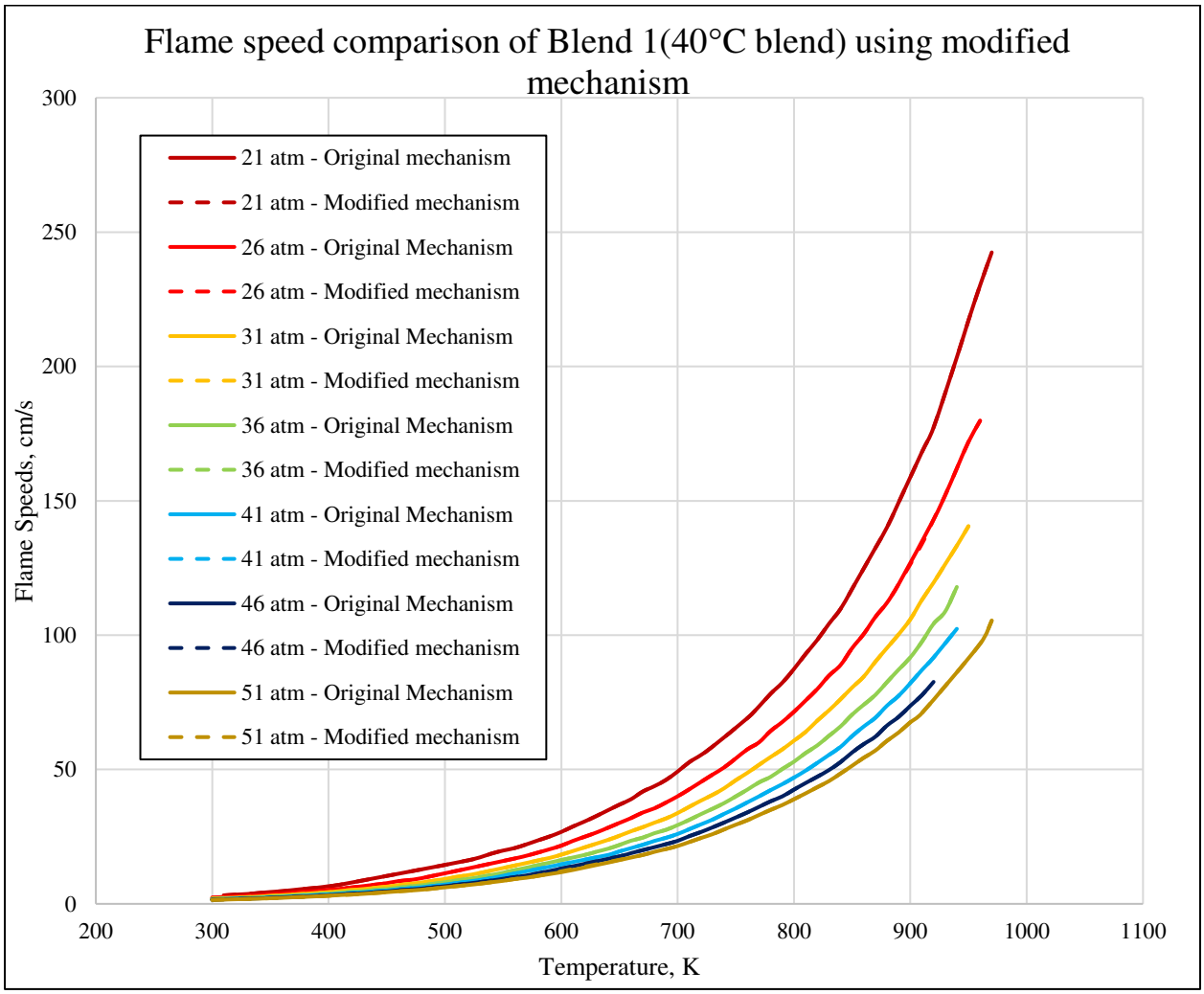


**FIGURE A2.1**: Comparison of flame speeds obtained from CHEMKIN with and without the OH* species in the chemical mechanism for Blend 1 (2.45 mol% $H_2O$)

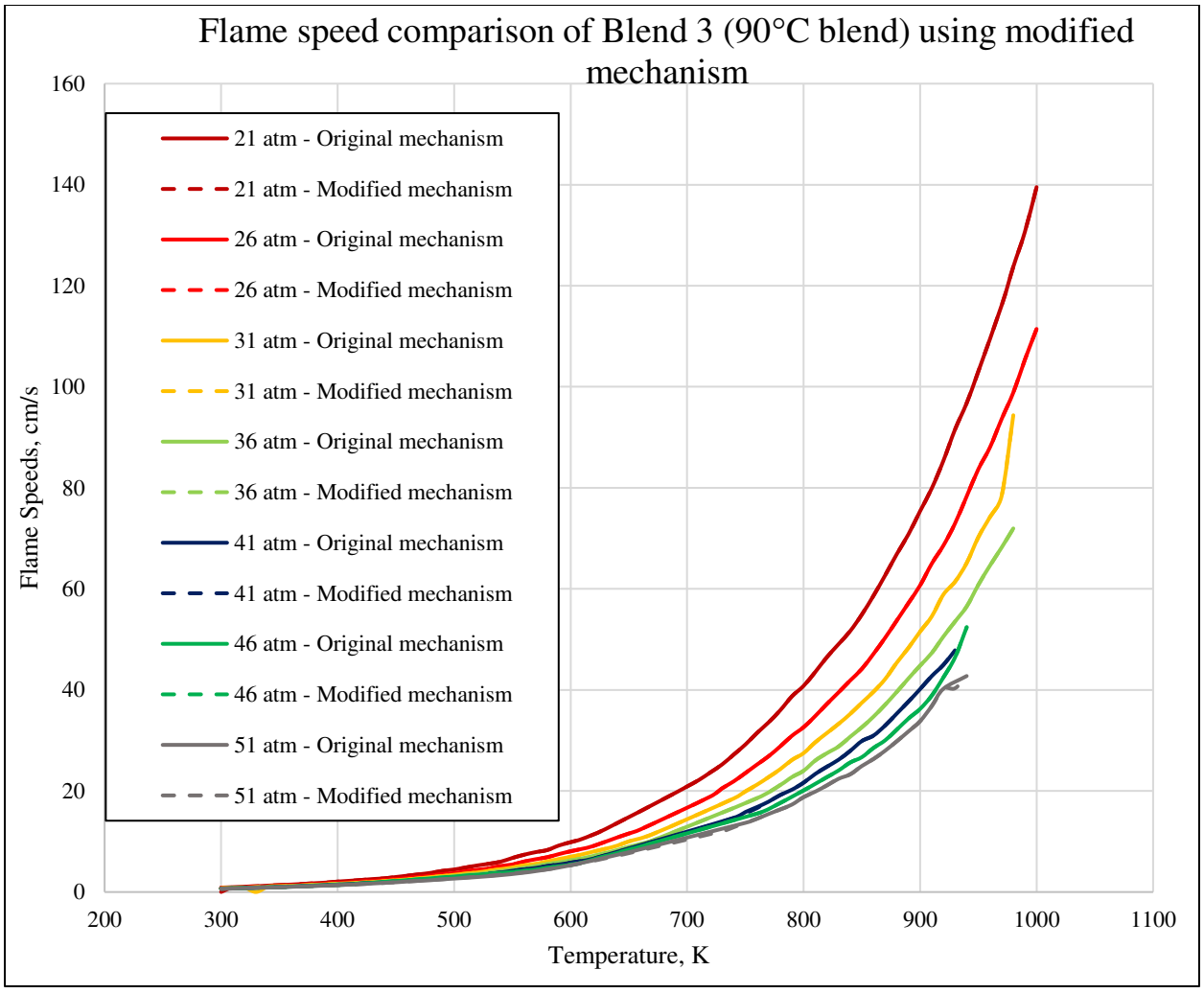


**FIGURE A2.2**: Comparison of flame speeds obtained from CHEMKIN with and without the OH* species in the chemical mechanism for Blend 3 (23.3 mol% $H_2O$)

# Appendix 3

During the TPA modelling, to match the predicted pressure trace with the experimentally measured pressure trace different multipliers pertaining to the heat transfer and valve flow area in the CFR model were adjusted. The TABLE A3.1 and A3.2 show the variables changed and the final values used in the model. Since the NUIG-syngas mechanism did not have any methane reactions in it, the intake composition was slightly changed to account for the absence of the species. Since the combustion model requires initialization data from the TPA model, the different TPA runs with the modified intake compositions were conducted for use in the combustion model using the NUIG-syngas mechanism and the averaged multipliers are tabulated below.

**TABLE A3.1**: Average value of multipliers used for the TPA runs for Blend 1 (40°C blend) when the different mechanisms were to be used

| | **Value when composition used for SD and GRI mechanisms** | **Value when composition used for NUIG mechanisms** |
|---|---|---|
| **Intake flow area multiplier** | 1 | 1 |
| **Exhaust Flow Area Multiplier** | 0.9 | 0.9 |
| **In-cylinder convection multiplier** | 0.8 | 0.8 |
| **Intake port heat transfer multiplier** | 1.66 | 1.66 |
| **Exhaust port heat transfer multiplier** | 1.5 | 1.5 |

**TABLE A3.2**: Average value of multipliers used for the TPA runs for Blend 3 (90°C blend) when different mechanisms were to be used

| | **Value when composition used for SD and GRI mechanisms** | **Value when composition used for NUIG mechanisms** |
|---|---|---|
| **Intake flow area multiplier** | 1.2 | 1.2 |
| **Exhaust Flow Area Multiplier** | 1 | 1 |
| **In-cylinder convection multiplier** | 0.846875 | 0.7 |
| **Intake port heat transfer multiplier** | 1.07 | 1.07 |
| **Exhaust port heat transfer multiplier** | 1 | 1 |